NASA Contractor Report 189086

A Geometric Nonlinear Degenerated Shell Element Using a Mixed Formulation With Independently Assumed Strain Fields

Wiley E. Graf
University of Akron
Akron, Ohio

December 1991

Prepared for
Lewis Research Center
Under Grant NAG3–307

National Aeronautics and
Space Administration

ABSTRACT

A mixed formulation is chosen to overcome deficiencies of the standard displacement-based shell model. Element development is traced from the incremental variational principle on through to the final set of equilibrium equations. Particular attention is paid to developing specific guidelines for selecting the optimal set of strain parameters. Included is a discussion of constraint index concepts and their predictive capability related to locking. Performance characteristics of the elements are assessed in a wide variety of linear and nonlinear plate/shell problems.

Despite limiting the study to geometric nonlinear analysis, a substantial amount of additional insight concerning the finite element modelling of thin plate/shell structures is provided. For example, in nonlinear analysis, given the same mesh and load step size, mixed elements converge in fewer iterations than equivalent displacement-based models. It is also demonstrated that, in mixed formulations, lower order elements are preferred. Additionally, meshes used to obtain accurate linear solutions do not necessarily converge to the correct nonlinear solution. Finally, a new form of locking was identified associated with employing elements designed for biaxial bending in uniaxial bending applications.

ACKNOWLEDGEMENTS

The author is deeply indebted and appreciative of the guidance, support and encouragement of Drs. Tse-Yung Chang and Atef F. Saleeb throughout the course of his graduate studies. Unquestionably, this research work would not have been possible without their help. Dr. Chang's assistance in helping secure employment upon graduation is also gratefully acknowledged.

The author also wishes to express his appreciation to the remainder of his Doctoral Committee - Drs. Joseph Padovan, David N. Robinson and Phillip H. Schmidt - for their suggestions and comments over the past few years.

The support of NASA Lewis Research Center, and Dr. C.C. Chamis in particular, is also acknowledged. Dr. Chamis was responsible for a good portion of the author's financial assistance while attending graduate school.

Dr. Krich Sawamiphakdi's input is recognized as well. His previous investigations and code development for the standard displacement-based element provided the starting point for this research.

The support of fellow graduate students Drs. Steven Arnold, Joseph Recktenwald, Matthew Eckert and faculty member Dr. Mark Kennedy is similarly noted.

The contributions of Ziza Saleeb are also acknowledged. She is responsible for the artwork that went into preparing the figures contained herein.

TABLE OF CONTENTS

LIST OF TABLES

LIST OF FIGURES

CHAPTER 1

INTRODUCTION

1.1 Statement of Problem

A shell may be defined as being a curved structure in three-dimensional space having small thickness relative to its other two dimensions. Further classification as "thick" or "thin" is determined by the ratio of the shell's smallest radius of curvature to its thickness. Typical examples encountered in practice might include: (i) civil engineering arch and dome structures, (ii) aeronautics, with its aircraft and space structures, and (iii) sheet metal forming operations common to many engineering disciplines.

It is the accurate representation of these thin shell structures using the finite element method that has long been a concern of researchers. Understandably, in light of the vast number of real-world structures classifiable as shell-like, the development of such an element has received considerable attention.

These shell element formulations may be identified as falling into one of three distinct categories: (1) flat element assemblages, (2) intrinsic curved elements derivable from some specific shell theory, and (3) degenerated models (and their predecessors, the 3D solids). Each of these

approaches has certain advantages and limitations. The degenerated element has, however, gained the widest acceptance due largely to its generality which, among other things, enables it to be more easily extended for nonlinear analysis.

Despite its appeal, the degenerated element, in its most fundamental form, is far from trouble-free [32,48]. In particular, it has been observed to be: (i) susceptible to locking (both membrane and shear), (ii) sensitive to distortion, and (iii) lacking insofar as stress calculations are concerned.

In response to these shortcomings, numerous remedies have been proposed. Some of the more notable ones include reduced/selective integration [27,30,31,33,37,40,44,46,47, 48,56,62,66,72], heterosis models [32,34], stabilization techniques [10,11,13,39], discrete Kirchhoff elements [5, 8,9,22,23,36], and assumed strain methods [6,7,24,29,35,41, 49,55,65].

There is, however, still no general consensus in favor of a particular approach due to its inherent limitations. For instance, reduced/selective integration elements may, under certain loading and/or boundary conditions, trigger zero-energy deformation modes. Stabilization techniques involve certain parameters which still lack appropriate physical interpretations, while discrete Kirchhoff elements are applicable only in thin

plate/shell analysis. Finally, the assumed strain approach, while very successful in the treatment of transverse shear for straight-sided elements, does not appear to be readily extendable for the approximation of membrane strains in higher-order curved elements.

Departing from standard displacement-based formulations and their derivatives, various multifield element models, e.g. hybrid and mixed methods, have also been introduced [16,19,26,38,44,46,47,50,52,53,57-61,63,64, 67]. Comparatively, these models are much more sound theoretically. All energy contributions are included, as exact integration is used throughout. Additionally, this "gimmick-free" attribute of the multifield models enables them to be more easily extended for nonlinear analysis. Factors such as computational cost and need of specific guidelines for choosing appropriate strain (or stress) polynomials have contributed to their general lack of acceptance in the finite element community.

1.2 Intent of Present Work

The primary objective of this research is to extend the analysis capabilities of the 5 and 9-node linear mixed elements developed previously [19,61] to include geometric nonlinearities (large translations and rotations with small strains). Much of the theory described herein does in fact derive from these earlier formulations, e.g. the use of a modified Hellinger-Reissner principle, imposition of the

Mindlin/Reissner assumption, strain polynomial selection guidelines with accompanying constraint index arguments and finally, relaxation of the pointwise equilibrium requirement. The present development, of course, now takes into account nonlinear effects in the strain-displacement relations. Additionally, because of the iterative incremental step-by-step solution method employed, out-of-balance load considerations require that right-hand-side load terms also be included.

Having established the need for continued research into the thin shell finite element analysis area (Section 1.1), a discussion of the various methods presently available to improve performance of the standard element is taken up in Chapter 2. Assessing the strengths/weaknesses of each with regard to suitability for extension to nonlinear analysis, a degenerated mixed shell element is chosen.

A description of the element is given in Chapter 3. Much of the discussion mirrors that given in [19] and [61] related to development of the base linear element.

In an incremental fashion, Chapter 4 traces element development from the modified Hellinger-Reissner variational principle on through to the final set of equilibrium equations. Included are discussions addressing such items as: (i) comparison of stress and strain formulations, (ii) why an updated, rather than total Lagrangian approach is

preferred, (iii) energy-conjugate stress and strain measures, and (iv) why the "strain history" is needed in a mixed formulation even for a geometric nonlinear (elastic material) analysis.

Chapter 5 provides guidelines for selecting the appropriate strain polynomial. Again, much of the discussion here may also be found in earlier papers [19,61].

Implementation of the element into an existing finite element code is discussed in Chapter 6. This is included primarily to facilitate similar future developments involving new beam, plate or shell elements. It should also prove to be beneficial if the analysis capabilities of the existing element are extended at some later date.

Numerical studies designed to assess the behavioral characteristics of the element in a wide variety of linear and nonlinear plate/shell applications are presented in Chapter 7. Results are compared to those reported by other investigators using various plate/shell models as well as "exact" solutions, when available.

Chapter 8 begins with a brief summary of the research effort. Significant findings are also reported, along with suggestions for future research directions.

CHAPTER 2

REVIEW OF PREVIOUS WORK

As described in the previous chapter, there exist three distinct categories into which shell element formulations may fall. The degenerated element approach [1] does, however, provide a number of advantages and thus, is generally regarded as being the most attractive.

By applying appropriate constraints on the displacements (u,v,w) in conjunction with an interpolation scheme involving midsurface rotations as well as translations, a middle-surface element may be formulated, free of many of the shortcomings of previous theories. For instance, as a result of interpolating rotations separately from translations, only C^0-continuity is required of the kinematic variables, making the lower-order elements once again attractive. This approach is also appealing in that no consideration is given to any specific shell theory. The element thus may be used to analyze a wide variety of shell-type structures. Because transverse shearing deformations are included, the approach is equally valid for the analysis of thick shells. Finally, because of the ease in which the shell geometry and compatibility conditions may be

satisfied, extension to include the analysis of nonlinear shell problems should be straightforward.

Regardless of the approach, an efficient and reliable element for plate/shell analysis should satisfy certain criteria. In addition to convergence and invariant requirements [4,21,25,73], the element should be:

(i) Relatively simple in its formulation and application
(ii) Computationally efficient
(iii) Free of any zero-energy deformation modes
(iv) Free of shear/membrane locking
(v) Relatively insensitive to geometric distortions
(vi) Accurate insofar as stress predictions are concerned
(vii) Easily extendable for various types of nonlinear analysis

In general, it is rather difficult to achieve all of the characteristics listed above. The URI element, for example, is certainly simple and efficient, but may encounter difficulties under certain loading/boundary conditions, or if appreciably distorted. Mixed methods, on the other hand, can generally satisfy items (iii) - (vii)

but, relative to the URI element, require more effort computationally and are not as easily formulated.

With this general background in mind, some of the more successful degenerated plate/shell elements are reviewed. Discussion will focus on how effectively each of the formulations meet the above criteria, with particular attention given to item (vii).

2.1 Displacement-based Formulations

Assumed displacement models, obtained by invoking the stationarity of the total potential energy, represent the most frequently employed approach to formulating C^0 plate/shell elements. Despite their widespread use, these elements are, in certain applications, still quite inadequate. As a result, numerous alternative formulations have been introduced. In the following, some of the more popular methods for improving behavior of the standard element are described.

2.1.1 Reduced/Selective Integration Techniques

In terms of element modification, adoption of a uniform reduced integration scheme represents the most direct of all possible approaches. However, while the URI element may prove to be beneficial for its softening effects, under certain loading and/or boundary conditions, zero-energy deformation modes may develop. In this setting, the analysis becomes numerically unstable. Even more

dangerous is the formation of a near-mechanism. Here, the analysis remains stable, but yields a solution grossly in error.

Pugh et al [56] provides insight as to why these mechanisms form. A singularity parameter is defined by comparing the total number of available degrees of freedom to the total number of independent strain component equations. Inexact integration necessarily reduces the number of independent relations, thereby increasing the likelihood that a singularity may develop.

Of the five plate models investigated (4, 8, 9, 12 & 16-node), only the higher-order cubic element was free of locking when integrated exactly. None were mechanism-free when a uniform reduced integration rule was employed. Bathe and Bolourchi [3] in fact recommend the use of exactly integrated higher-order elements to combat locking since, in a general large displacement shell analysis, the effects of reduced integration have not as yet been accurately assessed. Their computational cost may, however, be excessive.

In the context of plate analysis, by underintegrating shear energy contributions only, the selective reduced integration elements are less susceptible to problems of rank deficiency. Applied to thin plates, the tendency to lock is also avoided. When extended to shells, however, the SRI element (shear only) was found to be of

little help [72]. Here, membrane contributions are of primary concern and they too must be evaluated with an integration scheme of reduced order. Though an improvement over the URI element, the number of zero-energy modes present in the SRI element (shear and membrane) may still be at an unacceptable level (see discussion to follow).

2.1.2 Heterosis Models

Focusing their attentions on the 9-node Lagrange plate element of [56], Hughes and his co-workers [31,32,34] proposed several schemes to improve its behavior. As had been previously reported by Pugh, this particular element locks when integrated exactly and introduces four zero-energy modes at element level if uniform reduced integration is used.

Initially, a selective reduced integration scheme was adopted [31]. The resulting element was lock-free and now contained only one zero-energy mode. Despite arguments that the remaining mode could usually be suppressed globally, it did still pose a potential danger, particularly when removed from the more easily understood domain of linear elastic isotropic analysis with unchanging boundary conditions. The heterosis element concept [32] eliminates this remaining mode by using only 8-node serendipity shape functions to describe transverse displacements, while retaining rotation effects at the interior node. This is

accomplished without greatly affecting the element's convergence characteristics (constraint index drops from 4 to 3).

The above was later extended for the general nonlinear case [34]. Throughout, "exact" integration was used for membrane contributions and satisfactory results were still obtained. This occurs only because each of the test problems considered were of the shallow shell variety where little, if any, significant membrane effects are felt. For deep shell analysis, it is necessary to underintegrate membrane terms as well, which then introduces three additional mechanisms [48].

Perhaps the most compelling feature of [34] was the introduction of a lamina system for defining the constitutive and strain-displacement relations. Since bending and membrane energies are coupled in a curved shell analysis, separation of their individual contributions had, in the past, posed a major problem. With this element-level reference frame, it is now possible to evaluate shear, bending and membrane energy contributions individually in a general nonlinear curved shell analysis, thus making the SRI elements much more attractive. It should be kept in mind, however, that even with this type of scheme (reduced integration on both shear and membrane), the 9-node Lagrange shell now contains not one (as with the plate element), but four kinematic modes at element level. Imposing the

heterosis model assumptions on transverse displacements only reduces the number of modes to three.

2.1.3 Stabilization Techniques

Potential rank deficiency problems in the URI element provide the motivation for stabilization techniques. The stabilizing parameters function to mitigate rank deficiency, while still retaining the beneficial softening effects of reduced integration. Being orthogonal to the rigid body and deformation modes, they are also observed to have no adverse effect on convergence. Early work [10] required the use of a free parameter to regulate the degree of stabilization. More recent efforts [39] identify these parameters as being related to generalized stresses/strains. To date, the nonlinear applications (geometric only) have not been severe. Extension into other more complex areas, with appropriate physical interpretation for the stabilizing parameters, is not clear.

2.1.4 Discrete Kirchhoff Elements

Misrepresentation of shear strain energy in the thin plate problem provides the motivation for Discrete Kirchhoff Element formulations. Here, locking is avoided by simply neglecting energy associated with transverse shear. This, of course, limits their use to thin plate/shell applications only, where shear strain energy is indeed negligible. Crisfield [22] later developed a set of constraint relations

associated with the neglecting of transverse shear strain energy. Again, extension for general nonlinear applications is not readily apparent.

2.1.5 Assumed Strain Formulations

Assumed strain formulations were introduced in response to the standard displacement-based element's inability to accurately represent certain strain energy contributions. The QUAD4 element [40] employs exact integration for bending response, but requires an assumed strain approach in conjunction with an SRI scheme for transverse and membrane shear. A free parameter related to the element's aspect ratio, and definition of a "residual bending flexibility" parameter are also required.

The assumed strain elements, while very successful in the treatment of transverse shear for straight-sided elements, experience difficulties when approximating membrane strains in higher-order curved elements. Some of the more recent formulations [7,55,65] have had success in simpler nonlinear applications.

2.1.6 Other Displacement-based Procedures

Of course, there have been many other approaches adopted in an attempt to improve upon those areas in which the standard displacement-based element has been observed to be deficient. The preceding sub-sections concentrated on only some of the more popular methods. Other procedures of

note include anisoparametric interpolation [68,69], physical lumping processes [2], mode decomposition [12,14], incompatible elements [71] and free-form finite element formulations [15].

2.2 Multifield Methods

As an alternative to the displacement method, various multifield approximations, e.g. hybrid, mixed and quasi-conforming models [67,70] may also be used for development of effective plate/shell elements. In the hybrid and mixed methods, for example, one has the freedom to approximate more than one field, e.g. displacements and stress (or strain), within an element. These methods appear to have greater potential, particularly for use in constrained media problems.

Applications of the hybrid and mixed methods to plate and shell analysis have had only limited success, for several reasons. First, relatively few studies have been undertaken, compared to the displacement-based models. Secondly, many of these previous investigations have failed to obtain reliable lower-order elements. Attentions were thus turned to the higher-order elements, for which the hybrid and mixed methods become less attractive. Additionally, in many of these earlier developments, pointwise equilibrium conditions were often imposed in selecting the assumed strain parameters [16,52-54,63,64]. This requirement places a severe limitation on the method's

usefulness, particularly in nonlinear applications. Finally, these methods suffer from a lack of specific guidelines for choosing appropriate stress (or strain) parameters. In fact, many previous studies were conducted on the basis of a trial-and-error procedure, in which numerical tests were performed to determine the "best" choice.

2.3 Element Selection/Justification

Having assessed the strengths/weaknesses of the various approaches available, a degenerated mixed shell element is chosen for the present research. The primary objective will be to extend the analysis capabilities of the 5 and 9-node linear elements developed previously [19,61] to include geometric nonlinearities.

As pointed out by Gallagher [25], the notion of reduced integration is not fully justifiable on theoretical grounds. The same might also be said of many of the other schemes cited in Section 2.1. The mixed element, on the other hand, is of sound theoretical basis. All energy contributions are included, since exact integration is used throughout. Additionally, this "gimmick-free" attribute enables mixed elements to be more easily extended for various nonlinear applications.

Even at the linear level, there are indications that mixed element formulations will be more successful in nonlinear analysis. Here, the mixed models, when compared

to the equivalent displacement-based element, were observed to be much less sensitive to distortion and substantially more accurate in evaluating stress [19,26,59-61]. This takes on added significance in nonlinear analysis, where : (i) even initially undistorted elements become distorted in highly geometric nonlinear settings, and (ii) the iterative solution process involves calculation of an out-of-balance load term, which is directly related to the element's current stress state. By being less sensitive to distortion and more accurate insofar as stress calculations are concerned, it follows that the mixed element, when compared to its equivalent displacement-based model, may converge in fewer iterations over the same size load step. Thus, the mixed element, despite requiring more effort to form the element stiffness matrix, quite possibly may be able to recover a large portion of this expense in a full-blown, nonlinear finite element analysis.

Finally, mixed element formulations are attractive due to their flexibility with regard to choosing the assumed strain polynomial. The "standard" elements have no such freedom, and are therefore more prone to locking. This is discussed more thoroughly in Section 5.2.

CHAPTER 3

ELEMENT DESCRIPTION

Set forth in this chapter is the methodology necessary to effectively track a typical shell element's location and subsequent deformation during an iterative step-by-step solution process. Inasmuch as the analysis is essentially a generalization of the linear case [19,61], information provided in these earlier works (also see [34]) is again made use of here.

3.1 Coordinate Reference Frames

To adequately describe position and motion of the shell, three separate Cartesian coordinate systems are required. These reference frames are illustrated in Figure 1 for the degenerated 9-node Lagrange shell element.

3.1.1 Global System

Typical of most formulations is a global system, defined in Figure 1 by the orthonormal base vectors $\underset{\sim}{e}_1$, $\underset{\sim}{e}_2$ and $\underset{\sim}{e}_3$. It functions to determine both the element geometry and its nodal translational degrees-of-freedom.

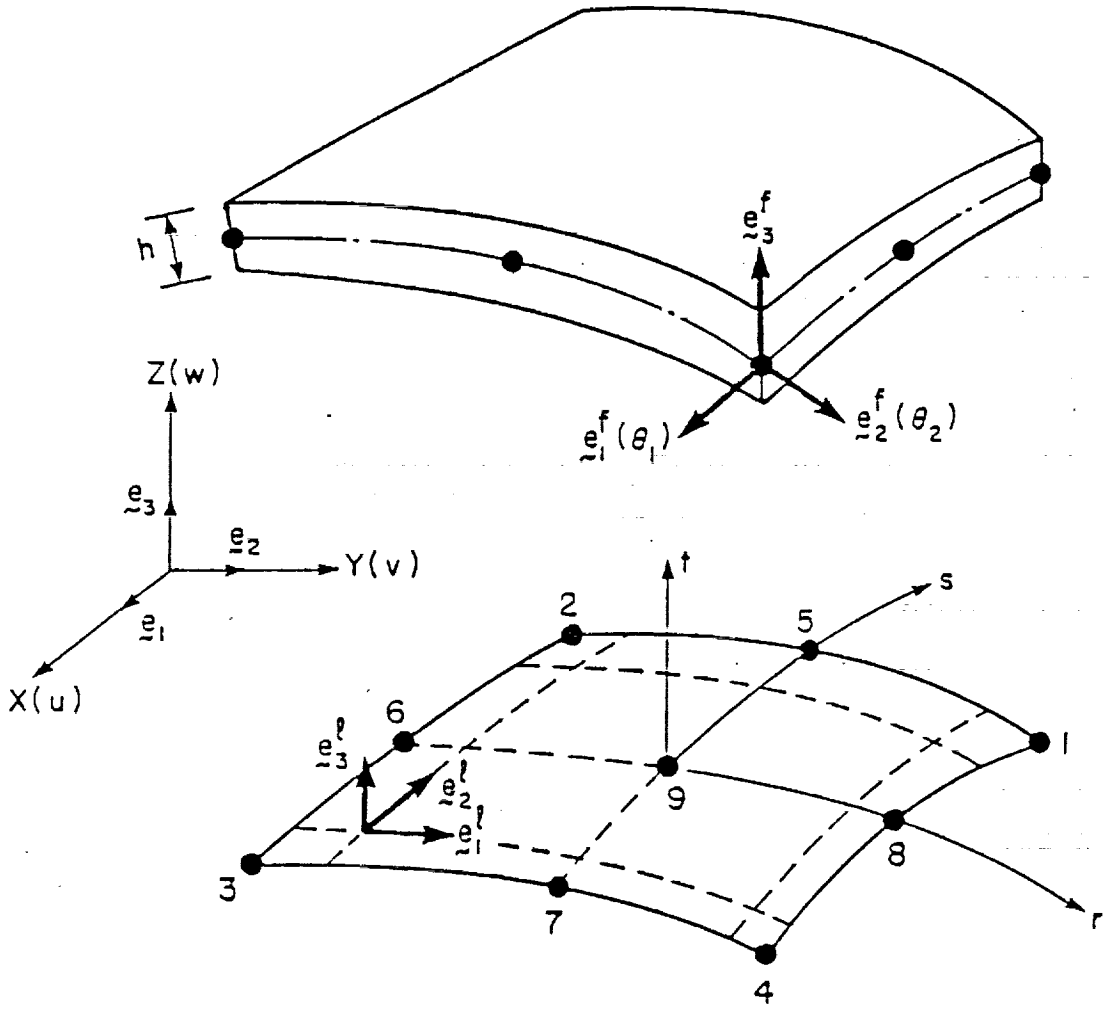

A Degenerated 9-Node Lagrange Shell Element
Figure 1

3.1.2 Fiber System

At each node, a unique local Cartesian reference frame is constructed. This fiber system, designated as $\underset{i}{e}^{f(k)}$, is used to define the nodal rotational degrees-of-freedom. To insure uniqueness at noncoplanar element intersections, the thickness direction must be defined (as user input) by specifying coordinates of the shell's top and bottom surfaces. At node "k" then,

$$\underset{3}{e}^{f(k)} = (\underset{k}{x}^{+} - \underset{k}{x}^{-}) / || \underset{k}{x}^{+} - \underset{k}{x}^{-} || \qquad (1)$$

where $\underset{k}{x} = (X,Y,Z)$ are the global Cartesian coordinates, and $|| \cdot ||$ the Euclidean norm of a vector. If coplanar, only middle surface geometry is required, with the fiber thickness direction specified as

$$\underset{3}{e}^{f(k)} = (\underset{k,r}{x} \times \underset{k,s}{x}) / || \underset{k,r}{x} \times \underset{k,s}{x} || \qquad (2)$$

where the comma denotes partial differentiation with respect to the indicated coordinate directions.

Regardless of the method chosen, once the fiber thickness is defined, specification of the two remaining fiber directions proceeds according to

$$\begin{aligned} \underset{1}{e}^{f(k)} &= \underset{2}{e} \times \underset{3}{e}^{f(k)} \\ \underset{2}{e}^{f(k)} &= \underset{3}{e}^{f(k)} \times \underset{1}{e}^{f(k)} \end{aligned} \qquad (3)$$

If the global Y-axis should happen to coincide with the fiber direction, $\underset{\sim}{e}_1^{f(k)}$ and $\underset{\sim}{e}_2^{f(k)}$ are defined instead as

$$\begin{aligned} \underset{\sim}{e}_2^{f(k)} &= \underset{\sim}{e}_3^{f(k)} \times \underset{\sim}{e}_1 \\ \underset{\sim}{e}_1^{f(k)} &= \underset{\sim}{e}_2^{f(k)} \times \underset{\sim}{e}_3^{f(k)} \end{aligned} \tag{4}$$

As the incremental analysis proceeds, this system rotates rigidly along with the nodal fiber. Fiber direction components are continually updated using a forward Euler method with a sufficiently large enough number of integration intervals (code default is 20), i.e.

$$\overset{t+\Delta t}{\underset{\sim}{e}}_3^{f(k)} = \overset{t}{\underset{\sim}{e}}_3^{f(k)} + \int \left(- \overset{t}{\underset{\sim}{e}}_2^{f(k)} \, d\theta_1^{(k)} + \overset{t}{\underset{\sim}{e}}_1^{f(k)} \, d\theta_2 \right) \tag{5}$$

where the left superscript is the time "variable" used to reference the current load step configuration. If iterations are required within the load step, "t" and "t+Δt" could then, of course, be replaced by iteration counters "i" and "i+1", with the equation being equally valid.

3.1.3 Lamina System

At each (r,s,0) integration point, a local Cartesian reference frame is defined such that two of its axes are tangent to the lamina (or middle) surface. This system, specified by three orthonormal base vectors $\underset{\sim}{e}_1^1$, $\underset{\sim}{e}_2^1$ and $\underset{\sim}{e}_3^1$, is constructed such that the in-plane laminae and natural coordinates share the same angular bisector (see Fig. 2)

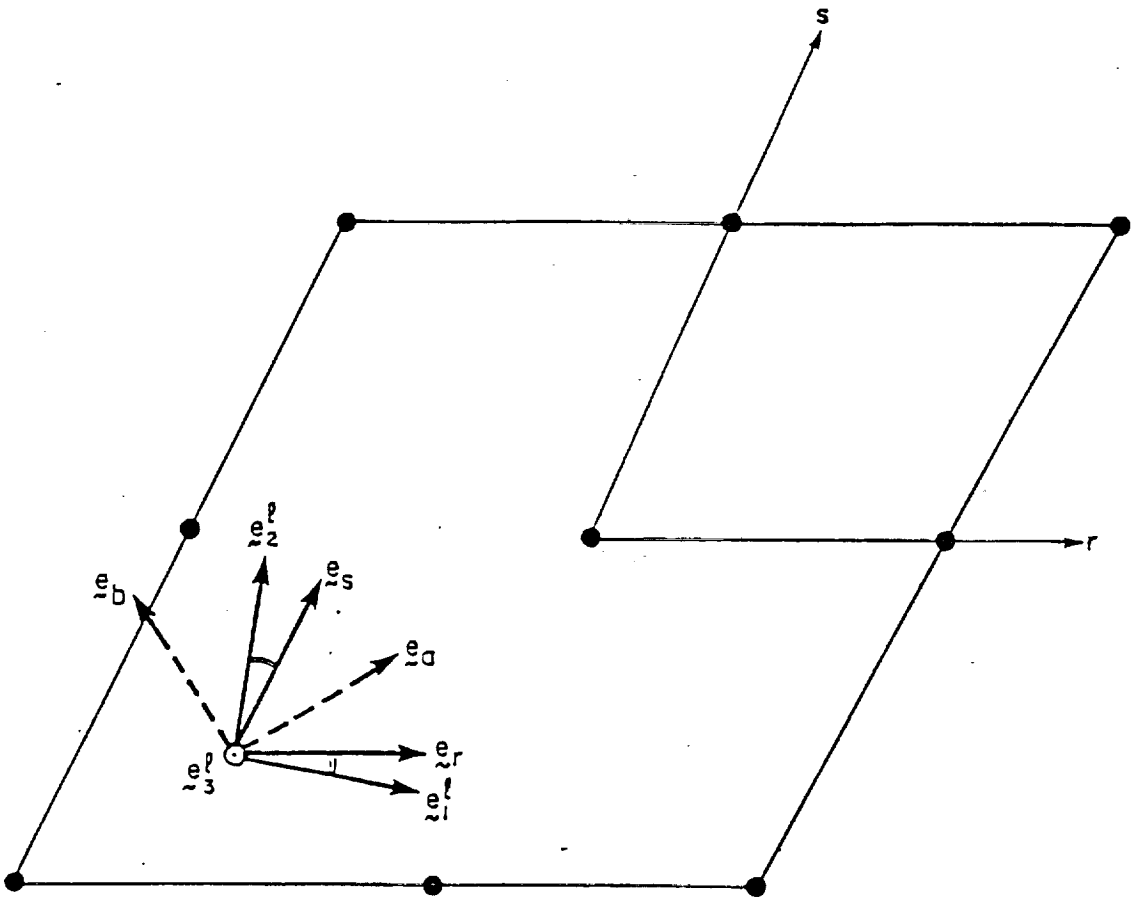

Lamina Coordinate System Construction (Plan View)
Figure 2

$$\underline{e}_r = \underline{x},r \;/\; ||\; \underline{x},r \;||$$

$$\underline{e}_s = \underline{x},s \;/\; ||\; \underline{x},s \;||$$

$$\underline{e}^1_3 = (\; \underline{e}_r \;\; x \;\; \underline{e}_s \;) \;/\; ||\; \underline{e}_r \;\; x \;\; \underline{e}_s \;||$$

$$\underline{e}_a = (\; \underline{e}_r + \underline{e}_s \;) \;/\; ||\; \underline{e}_r + \underline{e}_s \;|| \qquad (6)$$

$$\underline{e}_b = (\; \underline{e}^1_3 \;\; x \;\; \underline{e}_a \;) \;/\; ||\; \underline{e}^1_3 \;\; x \;\; \underline{e}_a \;||$$

$$\underline{e}^1_1 = (\; \underline{e}_a - \underline{e}_b \;) \;/\; ||\; \underline{e}_a - \underline{e}_b \;||$$

$$\underline{e}^1_2 = (\; \underline{e}_a + \underline{e}_b \;) \;/\; ||\; \underline{e}_a + \underline{e}_b \;||$$

Defining the lamina coordinates in this fashion is necessary in order to insure invariance of the stiffness matrix for nonrectangular elements. For the undistorted element, $\underline{e}^1_1$ and $\underline{e}^1_2$ degenerate to $\underline{e}_r$ and $\underline{e}_s$, respectively.

3.1.4 Additional Observations

As demonstrated for the 5-node element in Figure 3, $\underline{e}^1_3$ and $\underline{e}^f_3$, in general, do not coincide. In the first case, nonuniform element thickness causes $\underline{e}^1_3$ to deviate from the fiber direction. Figure 3(b) illustrates complications introduced when modelling shell-to-shell junctions. As a final example, the straight-sided quadrilateral simply cannot accurately define a curved geometry, which once again leads to a misalignment between $\underline{e}^1_3$ and $\underline{e}^f_3$. This, in fact, provides insight as to the proper procedure for generating

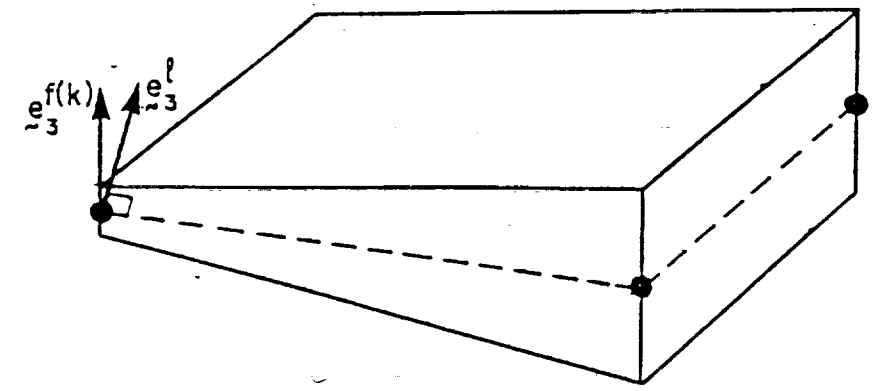

(a)

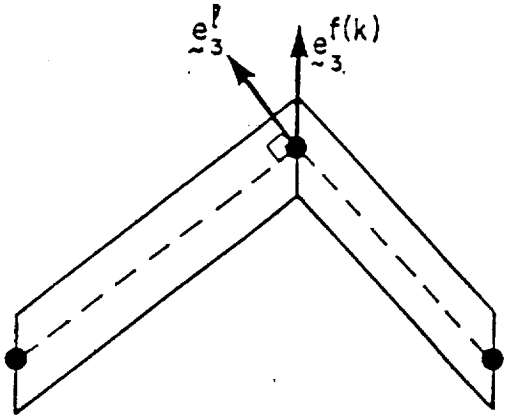

(b)

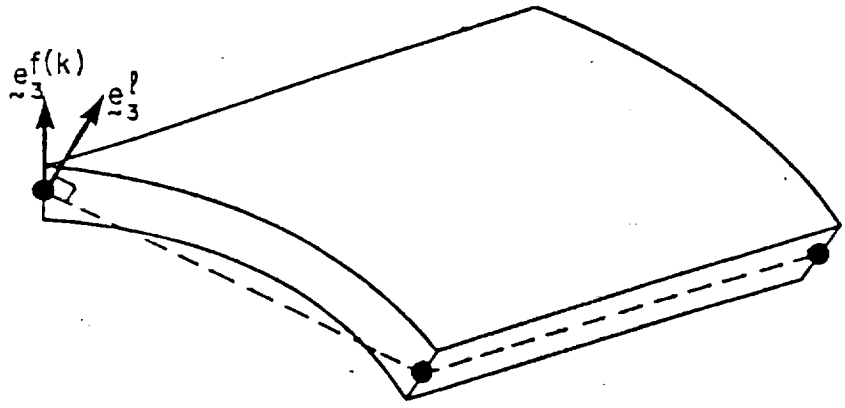

(c)

Misalignment of e_3^1 and the Fiber Direction

Figure 3

unique fiber reference frames. In general, equation (2) may be used for the 5-node element only if the initial geometry is flat. Similarly, for the 9-node element, if the structure may be defined geometrically by at most a second-order curve, (2) will generate identical fiber thicknesses for all elements sharing common nodes. Equation (1) would be applicable for more complex geometries. Of course, (1) should be used regardless, if either of the situations depicted in Fig. 3(a) or 3(b) exists.

Since the integration point-based lamina system rotates rigidly as the element deforms, it is also the most convenient for: (i) introducing the plane stress assumption, (ii) defining the constitutive relations, and (iii) interpolation of the assumed strain field. In this context, the strain-displacement operators, written in terms of global translational degrees-of-freedom, will naturally require a transformation if they too are to be represented in the lamina reference frame. This is accomplished by defining an orthogonal matrix $\underline{T}$ at each (r,s,0) integration point, i.e.

$$\underline{x} = \underline{T}\, \underline{x}^{1} \tag{7}$$

where $\underline{T}$ consists of direction cosines relating global and lamina coordinates. The transformation matrix defined above may then be used to obtain strain components with respect to the current lamina reference frame.

3.2 Geometric Description

The elements considered in this work are the nonlinear counterparts of [19] and [61], i.e. the 5-node quadrilateral and 9-node curved shell elements, which for later discussion are designated here as SHELM5 and SHELM9, respectively. As before, these elements are basically degenerated shells except that both displacement and strain fields are independently assumed. Even though top and bottom surfaces may have been used in specifying the fiber direction, in all other respects the elements are still considered middle surface models.

Consistent with the isoparametric formulation, position of a generic point in the element is defined in terms of natural coordinates as

$$\underset{\sim}{x}(r,s,t) = \sum_{k=1}^{n} N_k \underset{\sim}{x}_k + \frac{t}{2} \sum_{k=1}^{n} h_k N_k \underset{\sim}{e}_3^{f(k)} \qquad (8)$$

where, n = number of nodes used to describe element geometry

$\underset{\sim}{x}_k$ = position vector of nodal point "k" on the reference surface

h_k = shell thickness in fiber direction at node "k"

and N_k are the two-dimensional shape functions associated with node "k". The usual interpolations [4,21,73] still apply for SHELM9, with those of [61] again used here for the 5-node quadrilateral

$$N_5(r,s) = (1 - r^2) * (1 - s^2)$$

$$N_k(r,s) = \frac{1}{4}(1 + r\,r_k) * (1 + s\,s_k) - \frac{1}{4}N_5(r,s) \qquad (9)$$

In keeping with the linear element formulation, for SHELM5, only coordinates of the corner nodes (n=4) are used to define geometry in the initial configuration. However, as the solution proceeds, all five nodes are utilized in defining both $\underset{\sim}{x}$ and $\underset{\sim}{u}$.

Also of note is that equations (1)-(4) and (8) together uniquely map a biunit cube into the physical shell domain. Thus, for a fixed pair of (r,s) values, the line obtained from (8) corresponds to a fiber. A lamina surface results if "t" is held constant.

3.3 Kinematic Description

At each node, five degrees of freedom are defined; three translations (u,v,w) along the global Cartesian axes and two rotations $\theta_1^{(k)}$ and $\theta_2^{(k)}$ about mutually perpendicular axes $e_1^{f(k)}$ and $e_2^{f(k)}$ normal to the fiber thickness direction (see Figure 1). Elements SHELM5 and SHELM9 thus contain a total of 25 and 45 degrees-of-freedom, respectively.

Motion is defined by adopting the usual kinematic assumptions for degenerated element models: (i) Mindlin/ Reissner plate theory applies, thus enabling shear deformation effects to be included in the analysis, (ii) plane stress conditions prevail, so that no transverse normal stress is developed, and (iii) incrementally,

rotations are small (embedded in (5) also). With the above assumptions, element matrices can be formulated directly using standard isoparametric element procedures.

Considering (8) at times "0", "t" and "t+Δt", expressions for total and incremental displacements for a generic point in the element are given as

$$\underset{\sim}{u} = \sum_{k=1}^{n} N_k \, {}^{t}\underset{\sim}{u}_k + \frac{{}^{t}}{2} \sum_{k=1}^{n} h_k N_k \left({}^{t}\underset{\sim}{e}_{3}^{(k)} - {}^{0}\underset{\sim}{e}_{3}^{(k)} \right) \qquad (10)$$

$$\Delta\underset{\sim}{u} = \sum_{k=1}^{n} N_k \, \Delta\underset{\sim}{u}_k + \frac{{}^{t}}{2} \sum_{k=1}^{n} h_k N_k \left({}^{t+\Delta t}\underset{\sim}{e}_{3}^{(k)} - {}^{t}\underset{\sim}{e}_{3}^{(k)} \right) \qquad (11)$$

where, $\underset{\sim}{u}_k$ = translation of nodal point "k" referred to the element midsurface $\left({}^{t}\underset{\sim}{x}_k - {}^{0}\underset{\sim}{x}_k \right)$

$\Delta\underset{\sim}{u}_k$ = incremental translation of nodal point "k" referred to the element midsurface $\left({}^{t+\Delta t}\underset{\sim}{x}_k - {}^{t}\underset{\sim}{x}_k \right)$

with all other variables defined as before. Substituting the linearized approximation for (5) into (11), incremental displacements within an element may now be described in terms of the nodal point incremental translations and rotations

$$\Delta\underset{\sim}{u} = \sum_{k=1}^{n} N_k \, \Delta\underset{\sim}{u}_k + \frac{{}^{t}}{2} \sum_{k=1}^{n} h_k N_k \left(-{}^{t}\underset{\sim}{e}_{2}^{(k)} \, \theta_1^{(k)} + {}^{t}\underset{\sim}{e}_{1}^{(k)} \, \theta_2^{(k)} \right) \qquad (12)$$

The finite element solution will yield the nodal point variables $\Delta\underset{\sim}{u}_k$, $\theta_1^{(k)}$ and $\theta_2^{(k)}$, which are then substituted back into (5) to accurately define the current updated fiber system [4].

Utilizing (10) and (12), expressions for the global strain-displacement relationships can be written as

$$\underset{\sim}{e}^g = \partial \underset{\sim}{u} / \partial \underset{\sim}{x} = \underset{\sim}{B}_{NL}^g \, \underset{\sim}{q} \tag{13}$$

$$\Delta\underset{\sim}{e}^g = \partial \Delta\underset{\sim}{u} / \partial \underset{\sim}{x} = \underset{\sim}{B}_{L}^g \, \Delta\underset{\sim}{q} \tag{14}$$

where, $\underset{\sim}{e}^g$, $\Delta\underset{\sim}{e}^g$ = initial (time "t") and incremental global strains ordered as

$$(e_X, e_Y, e_Z, \gamma_{XY}, \gamma_{YZ}, \gamma_{XZ})^T$$

$\underset{\sim}{B}_L^g$, $\underset{\sim}{B}_{NL}^g$ = linear and nonlinear global strain-displacement operators (p. 377 of [4])

$\underset{\sim}{q}$, $\Delta\underset{\sim}{q}$ = initial and incremental nodal displacements ordered as

$$[u_1, v_1, w_1, \theta_1^{(1)}, \theta_2^{(1)}, \ldots u_n, v_n, w_n, \theta_1^{(n)}, \theta_2^{(n)}]^T$$

$[\,]^T$ = transpose of a row vector

The transformation defined in (7) may then be employed to obtain strain components referred to lamina coordinates. As described in Chapter 4, this is the preferred system in which to define the requisite finite element equations.

CHAPTER 4

FINITE ELEMENT FORMULATION

Finite element methods in structural and solid mechanics are frequently formulated via a variational approach. This chapter traces the element development from an incremental modified Hellinger-Reissner principle on through to the final set of finite element equilibrium equations. The variational is termed "modified" because a strain assumption is employed. Although equivalent to the stress formulation in linear analysis, a strain assumption does offer distinct advantages for nonlinear applications. For example, in the case of material nonlinearity, the bending strains may still be assumed to vary linearly in the shell thickness direction. This is certainly no longer true for the corresponding stress components. Moreover, material models residing in existing displacement-based finite element programs can still be utilized for the mixed methods without major coding modifications.

With respect to the finite element approximation for strain, decisions must be made regarding: (i) the reference frame to which the strain components are to be defined, and (ii) the coordinates in terms of which the polynomial basis functions for these strains are written. Although any

reference frame could be used (global, local, curvilinear), lamina coordinates are preferred because they are the most natural system in which to define the shell constitutive relations together with the zero normal shell stress assumption. To achieve the necessary element invariant property, strain polynomials interpolated in global Cartesian coordinates must be complete. This requirement would, however, negate one of the mixed model's most attractive features; namely, the freedom to judiciously select shear strain parameters to alleviate locking. Expressing in terms of natural coordinates instead, the invariance requirement is easily satisfied. In the derivations that follow then, a lamina system reference frame with strain polynomials expressed in natural (isoparametric) coordinates is implied.

Included in the formulation are nonlinear effects stemming from large displacements. In dealing with geometric nonlinearities, a total (TL) or updated (UL) Lagrangian approach may be used to describe the state of deformation. TL formulations refer all static and kinematic variables to an initial configuration at time "0", while an UL approach uses the previously calculated equilibrium configuration at time "t" as its reference. Both incorporate all kinematic nonlinear effects due to large displacements, rotations and strains so that, in theory, identical results should be obtained regardless of the

method chosen. In the present context, use of a rotating integration point-based lamina reference frame suggests an UL formulation might be the more efficient approach.

Finally, the issue of strain history for geometric nonlinear analysis must be addressed. In displacement-based element formulations, the strain (and therefore stress) at a point at any time "t" is obtained simply by differentiating the total displacement. This is not the case in a mixed formulation, however, where strains are interpolated incrementally. To determine the total strain at any time "t", it is therefore necessary to sum and store incremental strains at the integration points throughout the entire solution process. For material nonlinear analysis, of course, even the standard element requires some type of strain/stress history. This aspect of the formulation is further discussed in Chapter 6.

4.1 Incremental Modified Hellinger-Reissner Variational Principle

Although the functional outlined below may be used for large deflection, large strain analysis, the current research is confined to small strain applications. Provided an appropriate incremental strain energy potential can be defined, material nonlinear effects may also be incorporated.

With regard to the specific nature of the strain tensor, an UL formulation requires use of Almansi (total at

time "t") and updated Green (incremental) strains. The energy-conjugate stresses are then the Cauchy and updated 2nd Piola-Kirchhoff stresses, respectively [70].

As with any incremental step-by-step solution, the static and kinematic variables in some equilibrium configuration at time "t" are assumed to be known, with the objective being to determine their values in some unknown equilibrium configuration at time "t + Δt". A modified Hellinger-Reissner variational principle [51] provides the starting point for the incremental analysis:

$$\Delta\Pi_{HR}(\Delta\underline{u},\Delta\underline{e}) = \int_V [-1/2\ \Delta\underline{e}^T \underline{C}\ \Delta\underline{e} + (\underline{e} + \Delta\underline{e})^T \underline{C}\ \Delta\hat{\underline{e}} - \Delta\underline{e}^T \underline{C}\ (\underline{e} - \hat{\underline{e}}) - (\underline{F} + \Delta\underline{F})^T \Delta\underline{u}]\ dV - \int_{S_\sigma} [(\overline{\underline{T}} + \Delta\overline{\underline{T}})^T \Delta\underline{u}]\ dS - \int_{S_u} [\Delta\underline{T}^T (\Delta\underline{u} - \Delta\overline{\underline{u}} + \underline{u} - \overline{\underline{u}}) + \underline{T}^T \Delta\underline{u}]\ dS \quad (15)$$

where, $\underline{u}$, $\Delta\underline{u}$ = initial and incremental element displacement

$\Delta\underline{e}$ = independently assumed element incremental updated Green strains (see eqtn. 24)

$\Delta\hat{\underline{e}}$ = element incremental updated Green strains derived from displacements

$\underline{e}$ = element strains at time "t" from assumed strains

$\hat{\underline{e}}$ = element Almansi strains at time "t" derived from displacements

$\underline{C}$ = material stiffness matrix ($\underline{\sigma} = \underline{C}\underline{e}$)

$\underline{F}$, $\Delta\underline{F}$ = initial and incremental element body forces

$\underline{T}$, $\Delta\underline{T}$ = initial and incremental element boundary tractions

$(\ )^T$ = transpose of a column vector

$(\bar{\ })$ = prescribed quantity

V = element volume

S_σ, S_u = portions of element boundary surface area S over which tractions and displacements are prescribed, respectively

$$(S_\sigma \cup S_u = S \ ; \ S_\sigma \cap S_u = 0)$$

Invoking the stationarity conditions of (15) with respect to variations in $\Delta\underline{u}$ and $\Delta\underline{e}$ yields the corresponding Euler equations. In indicial notation, they are expressed as

$$\underline{e} = \hat{\underline{e}} = 1/2\ (u_{i,j} + u_{j,i} - u_{k,i}\ u_{k,j}) \tag{16}$$

$$\Delta\underline{e} = \Delta\hat{\underline{e}} = 1/2\ (\Delta u_{i,j} + \Delta u_{j,i} + \Delta u_{k,i}\ \Delta u_{k,j}) \tag{17}$$

$$(\tau_{ij} + \Delta S_{ij}),j + [(\tau_{kj} + \Delta S_{kj})\ \Delta u_{i,k}],j + (F_i + \Delta F_i) = 0 \tag{18}$$

along with the associated boundary conditions on S_σ and S_u. Equations (16) and (17) are the strain-displacement compatibility relationships, while (18) represents the nonlinear

stress equilibrium condition. Here, the material stiffness matrix linking stress to strain has been substituted.

Lumping the body force and surface integral contributions into a single externally applied load term $\bar{Q}$, equation (15) is simplified to the following form

$$\Delta\Pi_{HR}(\Delta u,\Delta e) = \int_V [-1/2\ \Delta e^T C\ \Delta e + e^T C\ D_L(\Delta u) + e^T C\ D_{NL}(\Delta u) + \Delta e^T C\ D_L(\Delta u) - \Delta e^T C\ e + \Delta e^T C\ (D_L(u) + D_{NL}(u))]\ dV - \bar{Q}^T \Delta u \quad (19)$$

where those strains derived from displacements have been further classified according to linear and nonlinear derivative operators

$$\hat{e} = D_L(u) + D_{NL}(u) = 1/2\ (u_{i,j} + u_{j,i}) - 1/2\ u_{k,i}\ u_{k,j} \quad (20)$$

$$\hat{\Delta e} = D_L(\Delta u) + D_{NL}(\Delta u) = 1/2\ (\Delta u_{i,j} + \Delta u_{j,i}) + 1/2\ \Delta u_{k,i}\ \Delta u_{k,j} \quad (21)$$

and the higher order term, $\Delta e^T C\ D_{NL}(\Delta u)$, has been neglected.

It is worth noting again at this point, that (19) is with respect to the lamina coordinate system at time "t" so that each of the derivative operators, as well as the

independently assumed incremental strains and constitutive relations, are local in nature. Specifically, this implies a transformation from global Cartesian reference frame for (20) and (21), and a material stiffness matrix of the form:

$$\underset{\sim}{C} = E/(1-v^2) = \begin{bmatrix} 1 & v & 0 & 0 & 0 \\ v & 1 & 0 & 0 & 0 \\ 0 & 0 & (1-v)/2 & 0 & 0 \\ 0 & 0 & 0 & k(1-v)/2 & 0 \\ 0 & 0 & 0 & 0 & k(1-v)/2 \end{bmatrix} \qquad (22)$$

where, E = Young's modulus

v = Poisson's ratio

k = shear correction factor (assumed to be 5/6)

As discussed earlier, the independently assumed strains (see eqtn. 24) are interpolated in the current lamina coordinates and, as such, require no additional transformation.

Since displacement derivatives appear in the variational, continuity requirements necessitate their being at least C^o-continuous. The strains, on the other hand, require no differentiation and are therefore permitted to be discontinuous across element interfaces. Consequently, the strain parameters may be eliminated at element level, leading to a stiffness matrix formulation similar to the conventional displacement-based elements.

Finally, it is also of interest to note that compatibility mismatch terms are included in the

formulation. Solutions obtained using standard displacement models automatically satisfy this relation since, by definition, strains are computed as derivatives of displacements. Mixed methods, however, interpolate strains independently from displacements and may therefore violate this most important requirement. To minimize drifting of the solution, the mismatch terms must be retained.

4.2 Finite Element Approximation and Element Stiffness Matrix

In the finite element discretization, $\Delta\underline{u}$ is interpolated in terms of nodal displacements, while $\Delta\underline{e}$ is approximated by a set of generalized strain parameters

$$\Delta\underline{u} = \underline{N}\,\Delta\underline{q} \tag{23}$$

$$\Delta\underline{e} = \underline{P}\,\Delta\underline{\beta} \tag{24}$$

Substitution of (23) and (24) into (19) leads to

$$\Delta\overline{\Pi}_{HR}(\Delta\underline{q},\Delta\underline{\beta}) = -1/2\;\Delta\underline{\beta}^{T}\underline{H}\,\Delta\underline{\beta} + \underline{Q}_1^{T}\Delta\underline{q} + 1/2\;\Delta\underline{q}^{T}\underline{K}_{NL}\Delta\underline{q} + \Delta\underline{\beta}^{T}\underline{G}\,\Delta\underline{q} + \Delta\underline{\beta}^{T}(\underline{Z}-\underline{W}) - \underline{Q}^{T}\Delta\underline{q} \tag{25}$$

where,

$$\underline{H} = \int_V [\underline{P}^{T}\underline{C}\,\underline{P}]\,dV \tag{26}$$

$$\underline{G} = \int_V [\underline{P}^{T}\underline{C}\,\underline{B}_L]\,dV \tag{27}$$

$$\underline{K}_{NL} = \int_V [\underline{B}_{NL}^{T}\hat{\underline{\tau}}\,\underline{B}_{NL}]\,dV \tag{28}$$

$$\underline{Q}_1 = \int_V [\underline{B}_L^{T}\underline{C}\,\underline{e}]\,dV \tag{29}$$

$$\underline{Z} = \int_V [\underline{P}^T \underline{C} \hat{\underline{e}}] \, dV \tag{30}$$

$$\underline{W} = \int_V [\underline{P}^T \underline{C} \underline{e}] \, dV \tag{31}$$

$\underline{Q}$ = terms in $\bar{\underline{Q}}$ of (19) (32)

$\underline{B}_L$ = linear strain-displacement operator referred to lamina coordinates

$$(\underline{B}_L = \underline{T} \, \overset{g}{\underline{B}}_L) \tag{33}$$

$\underline{B}_{NL}$ = nonlinear strain-displacement operator referred to lamina coordinates

$$(\underline{B}_{NL} = \underline{T} \, \overset{g}{\underline{B}}_{NL}) \tag{34}$$

$$\hat{\underline{\tau}} = \begin{bmatrix} \tau_{11} \underline{I}_3 & & \\ \tau_{12} \underline{I}_3 & \tau_{22} \underline{I}_3 & \text{(symmetric)} \\ \tau_{13} \underline{I}_3 & \tau_{23} \underline{I}_3 & \tau_{33} \underline{I}_3 \end{bmatrix} ; \quad \underline{I}_3 = \begin{bmatrix} 1 & 0 & 0 \\ 0 & 1 & 0 \\ 0 & 0 & 1 \end{bmatrix} \tag{35}$$

Invoking the stationarity of (25) with respect to strain yields $\Delta\underline{\beta}$ in terms of $\Delta\underline{q}$

$$\Delta\underline{\beta} = \underline{H}^{-1} [\underline{G} \, \Delta\underline{q} + (\underline{Z} - \underline{W})] \tag{36}$$

The incremental strain parameters are eliminated at element level by substituting the above relation back into (25). After some manipulation, the functional reduces to

$$\Delta\Pi_{HR}(\Delta q) = 1/2\ \Delta q^T G^T H^{-1} G\ \Delta q + \Delta q^T G^T H^{-1} (Z-W)$$
$$+1/2\ (Z-W)^T H^{-1} (Z-W) + \Delta q^T Q_1$$
$$+1/2\ \Delta q^T K_{NL} \Delta q - \Delta q^T Q \qquad (37)$$

Stationarity of the functional, now with respect to Δq leads to

$$K\ \Delta q = Q - (Q_1 + Q_2) \qquad (38)$$

$$K = G^T H^{-1} G + K_{NL} \qquad (39)$$

$$Q_2 = G^T H^{-1} (Z-W) \qquad (40)$$

where K represents the element tangent stiffness matrix, and Q_2 an additional right-hand-side load vector contribution appearing as a result of including compatibility mismatch terms in the original variational statement. Any corrections for equilibrium mismatch are also intrinsically included in the formulation as Q_1 functions to balance internal stresses with external loads in the iterative solution process.

Solving for Δq in (38) leads to an approximation for the nodal point displacements at time "$t+\Delta t$", i.e.

$$q^{t+\Delta t} = q^t + \Delta q \qquad (41)$$

By inserting Δq back into (36), the corresponding incremental strains can be obtained from (24)

$$\Delta \underline{e} = \underline{P}\, \Delta \underline{\beta} = \underline{P}\, \underline{H}^{-1} [\underline{G}\, \Delta \underline{q} + (\underline{Z} - \underline{W})] \qquad (42)$$

Adding to those at time "t" yields an approximation to the total strains at time "t+Δt". Stresses are then directly obtained from (22) as

$$\underline{\sigma} = \underline{C}\, \underline{e} = \underline{C} \sum \Delta \underline{e} = \underline{C} \sum \underline{P}\, \underline{H}^{-1} [\underline{G}\, \Delta \underline{q} + (\underline{Z} - \underline{W})] \qquad (43)$$

However, because of the various assumptions and linearizations involved, such a solution may be subject to very significant errors. In practice therefore, it is usually necessary to iterate until a solution for $\Delta \underline{q}$ is obtained to "sufficient accuracy".

4.3 Recovering the Linear Element

The corresponding linear element may be recovered from (15) simply by assuming that all terms associated with initial effects vanish. For clarity, the "Δ 's" are dropped so that the functional for the linear element becomes

$$\prod_{HR}(\underline{u}, \underline{e}) = \int_V [-1/2\ \underline{e}^T \underline{C}\, \underline{e} + \underline{e}^T \underline{C}\, \hat{\underline{e}} - \underline{F}^T \underline{u}]\ dV - \int_{S_\sigma} [\overline{\underline{T}}^T \underline{u}]\ dS - \int_{S_u} [\underline{T}^T (\underline{u} - \overline{\underline{u}})]\ dS \qquad (15^*)$$

The above is further simplified, by again lumping the body force and surface integral contributions into a single externally applied load term

$$\prod_{HR}(\underline{u}, \underline{e}) = \int_V [-1/2\ \underline{e}^T \underline{C}\, \underline{e} + \underline{e}^T \underline{C}\, D_L(\underline{u})]\ dV - \overline{\underline{Q}}^T \underline{u} \qquad (19^*)$$

In the finite element discretization, $\underline{u}$ is interpolated in terms of nodal displacements, while $\underline{e}$ is approximated by a set of strain parameters

$$\underline{u} = \underline{N}\,\underline{q} \tag{23*}$$

$$\underline{e} = \underline{P}\,\underline{\beta} \tag{24*}$$

Substitution of (23*) and (24*) into (19*) leads to

$$\Pi_{HR}(\underline{q},\underline{\beta}) = -1/2\ \underline{\beta}^{T}\,\underline{H}\,\underline{\beta} + \underline{\beta}^{T}\,\underline{G}\,\underline{q} - \underline{Q}^{T}\,\underline{q} \tag{25*}$$

where $\underline{H}$, $\underline{G}$ and $\underline{Q}$ have been defined previously in (26), (27) and (32). As before, the stationarity of (25*) yields $\underline{\beta}$ as a function of $\underline{q}$

$$\underline{\beta} = \underline{H}^{-1}\,\underline{G}\,\underline{q} \tag{36*}$$

The strain parameters are eliminated at element level by substituting $\underline{\beta}$ back into (25*). Variation of the resulting functional leads to

$$\underline{K}\,\underline{q} = \underline{Q} \tag{38*}$$

where the stiffness for the linear element is given by

$$\underline{K} = \underline{G}^{T}\,\underline{H}^{-1}\,\underline{G} \tag{39*}$$

Once the nodal point displacements $\underline{q}$ have been calculated, the corresponding strains are obtained from (36*) and (24*)

$$\underline{e} = \underline{P}\,\underline{\beta} = \underline{P}\,\underline{H}^{-1}\,\underline{G}\,\underline{q} \qquad (42^*)$$

Element-aligned stresses are then recovered using the stress-strain relation defined in (22)

$$\underline{\sigma} = \underline{C}\,\underline{e} = \underline{C}\,\underline{P}\,\underline{H}^{-1}\,\underline{G}\,\underline{q} \qquad (43^*)$$

CHAPTER 5

STRAIN APPROXIMATION

Derivation of the nonlinear SHELM5 and SHELM9 elements is complete once the strain polynomial functions, i.e. entries of $\underline{P}$ in (24), are determined. This, in fact, is the most crucial point of the development. For example, if the polynomial chosen is of insufficient order, zero-energy modes may develop. At the other extreme, an excessive number of strain parameters will ultimately result in the element locking when used in constrained media applications.

In [19,61], several useful concepts and criteria proposed in the literature were assessed and synthesized in an attempt to develop a general framework for the selection procedure. It was concluded that, in general, four considerations should be given in choosing the strain polynomial functions: (i) all kinematic modes must be suppressed, (ii) constraint index must be greater than zero, (iii) element properties must be invariant, and (iv) whether or not the stress calculated from the assumed strain functions should satisfy the pointwise equilibrium requirement.

As in these earlier studies, here too, equilibrium is relaxed. The decision appears justified since, as demonstrated in (18), this requirement is in fact fulfilled, at least in an averaged integral sense. Moreover, the right-hand-side load vector term $\underset{\sim}{Q}_1$ indirectly enforces equilibrium as it "balances" internal stresses with the applied loads. The remainder of this chapter then will focus on items (i)-(iii) and their influence on the selection process.

5.1 Suppression of Zero-Energy Deformation Modes

A necessary requirement for the element stiffness matrix to be of sufficient rank is that the number of strain parameters should be greater than or equal to (d-r), where "d" is the total number of displacement degrees-of-freedom, and "r" the number of rigid body modes. Since multiple strain parameters may correspond to the same deformation mode leaving some degrees-of-freedom "unsuppressed", the above condition is certainly not sufficient to ensure proper rank. Based on considerations of deformation energy, it was further suggested in [54] that the total number of strain parameters should indeed be kept minimum, while simultaneously suppressing all kinematic deformation modes. Not only is this least-order approximation desirable with regard to constraint index arguments, but it is the most computationally efficient approach as well.

5.2 Locking and the Constraint Index

Because various deformation modes may activate more than one strain component, there is some flexibility with regard to the manner in which these modes are suppressed. Indeed, it is precisely this freedom in choosing the strain polynomial which enables the mixed element to filter out "troublesome" terms, thus alleviating locking. To illustrate, consider the degenerated plate/shell incremental strain-displacement relations expressed in natural coordinates

$$\hat{\Delta \underline{e}}_m = \begin{bmatrix} \frac{\partial \Delta u}{\partial r} \\ \frac{\partial \Delta v}{\partial s} \\ \frac{\partial \Delta u}{\partial s} + \frac{\partial \Delta v}{\partial r} \end{bmatrix} \tag{44}$$

$$\hat{\Delta \underline{e}}_b = \begin{bmatrix} \frac{\partial \Delta \theta r}{\partial r} \\ -\frac{\partial \Delta \theta s}{\partial s} \\ \frac{\partial \Delta \theta r}{\partial s} - \frac{\partial \Delta \theta s}{\partial r} \end{bmatrix} \tag{45}$$

$$\hat{\Delta \underline{\gamma}} = \begin{bmatrix} \frac{\partial \Delta w}{\partial s} - \Delta \theta_s \\ \frac{\partial \Delta w}{\partial r} + \Delta \theta_r \end{bmatrix} \tag{46}$$

Since displacement modes corresponding to $\Delta\theta_r$ and $\Delta\theta_s$ appear in both bending and shear strain expressions, to minimize constraints (shear), given a choice, $\Delta\beta$'s selected to suppress the $\Delta\theta_r$ and $\Delta\theta_s$ modes are assigned to the bending components.

The standard displacement-based element, of course, has no such flexibility. All displacement modes associated with $\Delta\theta_r$ and $\Delta\theta_s$ are carried along in the shear strain expression. This element naturally then is much more likely to lock as the plate/shell thickness becomes small.

Constraint index concepts provide the motivation for discussions such as the one above. As originally conceived [44], they were developed in an attempt to analytically gauge an element's behavior in some limiting case by relating deformation degrees-of-freedom to constraint relations. In equation form:

$$CI = NK - NC \tag{47}$$

where, CI = element constraint index

NK = number of kinematic degrees-of-freedom brought by an element when added to an existing mesh

NC = number of independent constraints introduced in the limiting case (thin plate in the present context)

The constraint index then is a measure of the "true degrees-of-freedom" brought to the finite element mesh. Positive values of CI suggest that the element will behave favorably, while CI $\leq$ 0 indicates failure in constrained media applications.

5.3 Element Invariance

As discussed in the previous chapter, natural coordinate representation of the strain polynomial is the most effective means of achieving the element invariant property. Also noted in Chapter 3 was the special treatment required in constructing the lamina coordinate reference frame. Specifically, the in-plane laminae and natural coordinates must share the same angular bisector (see Figure 2).

As a counter-example, assume that the lamina system is defined such that $\bar{e}_1$ (designated as $\hat{e}_1$ in Figure 4) is always directed along the natural coordinate r-axis. Figures 4(a) and 4(b) illustrate two of the four possible element numbering schemes. Because of the nonzero distortion angle θ, $\hat{e}_1$ in (a) rotates by only (90-θ) degrees if renumbered as in (b). Since renumbering implies a 90-degree rotation in the rs-plane (strains $\Delta e_{11}(r,s)$ and $\Delta e_{22}(r,s)$ are orthogonal) and $\hat{e}_1$ rotates only (90-θ) degrees, the invariant property is lost for all but the undistorted rectangular elements. The equal angle bisector approach

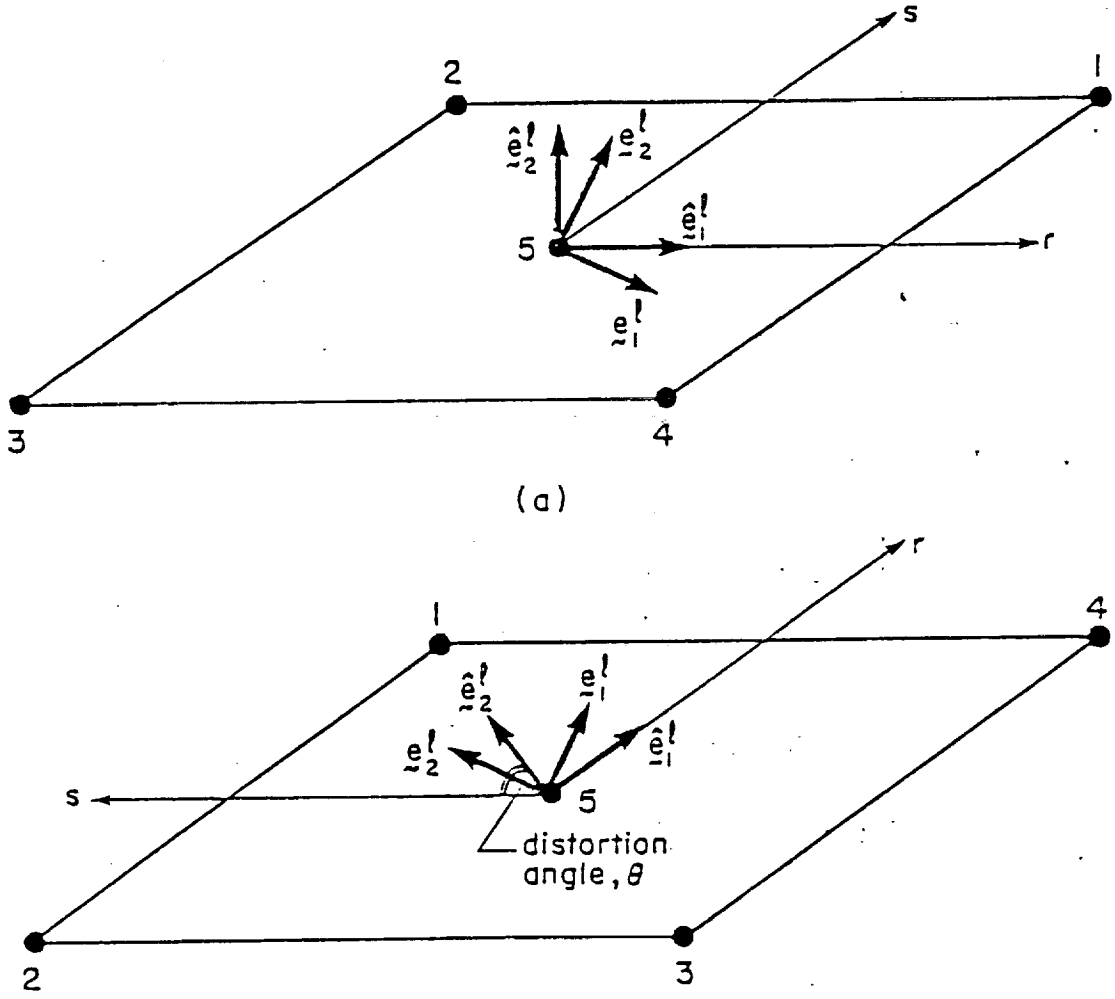

Invariance and the Lamina Coordinate Reference Frame
Figure 4

always rotates $\underset{\sim}{e}_i^1$ in 90-degree increments in the rs-plane regardless of the numbering scheme chosen.

The above is still not sufficient to guarantee invariance. Clearly, if the strain polynomial is not symmetric with respect to permutation of the "r" and "s" variables, the elements of Figure 4(a) and 4(b) would yield two distinctly different responses. To summarize, invariance is assured only if: (i) a balanced strain polynomial is used (e.g. for every s-term in Δe_{11}, there is a corresponding r-term in Δe_{22}) and (ii) it is written with respect to an equal angle bisector lamina system.

5.4 Strain Polynomial Functions

When considered together, the above guidelines lead to strain being approximated in terms of natural coordinates as

$$\Delta \underset{\sim}{e} = \begin{bmatrix} \underset{\sim}{P}_m & 0 & \underset{\sim}{P}_b \\ 0 & \underset{\sim}{P}_\gamma & 0 \end{bmatrix} * \begin{bmatrix} \Delta \underset{\sim}{\beta}_m \\ \Delta \underset{\sim}{\beta}_\gamma \\ \Delta \underset{\sim}{\beta}_b \end{bmatrix} \qquad (48)$$

where subscripts m, γ, and b refer to membrane, shear and bending, respectively. For SHELM5

$$\underset{\sim}{P}_m = \begin{bmatrix} 1 & r & s & 0 & 0 & 0 & 0 \\ 0 & 0 & 0 & 1 & r & s & 0 \\ 0 & 0 & 0 & 0 & 0 & 0 & 1 \end{bmatrix} \qquad (49)$$

$$\underset{\sim}{P}_{\gamma} = \begin{bmatrix} 1 & r & s & 0 & 0 \\ 0 & 0 & r & 1 & s \end{bmatrix} \tag{50}$$

and for SHELM9

$$\underset{\sim}{P}_{m} = \begin{bmatrix} 1 & r & s & rs & s^2 & rs^2 & 0 & 0 & 0 & 0 & 0 & 0 & 0 & 0 & 0 \\ 0 & 0 & 0 & 0 & r^2 & 0 & 1 & r & s & rs & sr^2 & 0 & 0 & 0 & 0 \\ 0 & 0 & 0 & 0 & 0 & 0 & 0 & 0 & 0 & 0 & 0 & 0 & 1 & r & s & rs \end{bmatrix} \tag{51}$$

$$\underset{\sim}{P}_{\gamma} = \begin{bmatrix} 1 & r & s & rs & sr^2 & 0 & 0 & 0 & 0 \\ 0 & 0 & 0 & 0 & rs^2 & 1 & r & s & rs \end{bmatrix} \tag{52}$$

with bending strains for both elements defined as

$$\underset{\sim}{P}_{b} = t * \underset{\sim}{P}_{m} \tag{53}$$

The above interpolations correspond exactly to those given in [61] and [19]. This is to be expected since the present study is a natural generalization of these earlier works.

Equations (49)-(53) represent a least-order approximation for strain which simultaneously suppresses all kinematic modes. It is easily verified that the invariant requirement is also satisfied. The constraint index and its predictive capability related to locking warrant further discussion, however.

Illustrated in Figure 5 are CI calculations for elements SHELM5 and SHELM9. Applied to the shear locking problem, no degradation in element performance is anticipated, as CI > 0 in both cases. However, once

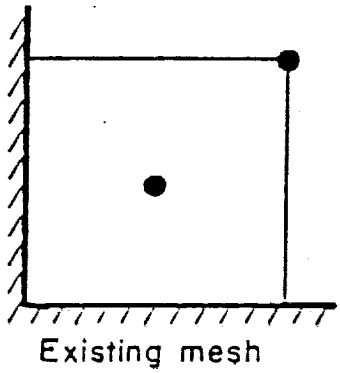

Shear (plate)	Shear + Membrane
NK = 6	NK = 10
NC = 5	NC = 12
CI = +1	CI = -2

(a) Element SHELM5

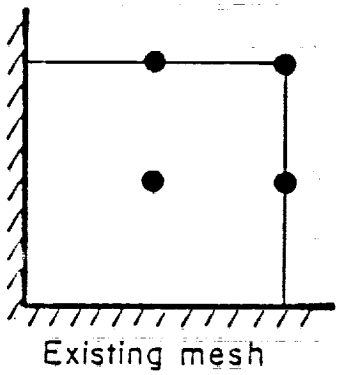

Shear (plate)	Shear + Membrane
NK = 12	NK = 20
NC = 9	NC = 24
CI = +3	CI = -4

(b) Element SHELM9

Constraint Index Calculations
Figure 5

membrane constraints are introduced, (47) suggests potential problems. It was argued in [19] that perhaps a direct application of the constraint index is too severe. Requiring $\Delta\underset{\sim}{\beta}_{\gamma}$ --> 0 is realistic because shear strain must vanish for thin plates/shells subject to transverse loading. But, since many shell problems of practical importance are dominated by membrane actions (and hence, $\Delta\underset{\sim}{\beta}_{m}$ is in fact nonzero and therefore should not be required to vanish), equation (47) is viewed as being overly pessimistic.

In light of the above discussion, apparently interpretation of the constraint index applied to shells is a much more difficult issue to deal with. Indeed, whether or not a constraint is active will depend upon the structure geometry and loading. Boundary restraints enter in as well, so that the constraint index is very much a problem-dependent quantity. Trouble-free performance is assured for nonnegative CI, since (47) represents a worst-case limiting criteria. However, CI $\leq$ 0 does not necessarily indicate failure, since it is not entirely realistic to think that all constraints will be active simultaneously.

5.5 Element Distortion Considerations

The elements considered may encounter two levels of distortion; namely, that due to: (i) curvature, and (ii) deviation from rectangular configuration in plan view. The integration point-attached rotating lamina system automatically incorporates the effects of curvature

throughout the entire deformation process. For elements skewed in the local rs-coordinates, the following covariant coordinate transformation is introduced

$$\underset{\sim}{e}^{1} = \underset{\sim}{J}^{T} \underset{\sim}{e} \underset{\sim}{J} \tag{54}$$

where, $\underset{\sim}{J}$ is the element centroidal Jacobian transformation matrix in the rs-plane relating lamina and natural coordinates. The constant (centroidal) Jacobian is essential to maintaining the order of the assumed strain polynomial. Evaluated otherwise might trigger the formation of kinematic modes or induce the locking problem once again.

The above transformation was not included in earlier formulations [58,61]. In [58], mesh distortions were compensative, so that the overall system response was not severely degraded. For unidirectional skewed problems (see [19], [45] and Section 7.2) however, special treatment is required in the form of (54) to reduce the element's sensitivity to distortion.

CHAPTER 6

IMPLEMENTATION

Described herein are the necessary modifications to attach elements SHELM5 and SHELM9 to an existing finite element analysis program. A research-oriented code, NFAP [17], is chosen, although the following discussion is appropriate to any general-purpose nonlinear finite element package. As has been earlier demonstrated, since strain parameters are eliminated at element level leaving only nodal displacements as unknowns, the mixed elements are made transparent from a user standpoint. Once in place, the user thus requires no additional information with regard to the underlying theory in order to effectively use these elements.

6.1 Program Flow

The overall program flow for NFAP is outlined in Figure 6, where those portions affected by the addition of elements SHELM5 and SHELM9 are indicated in boldface type.

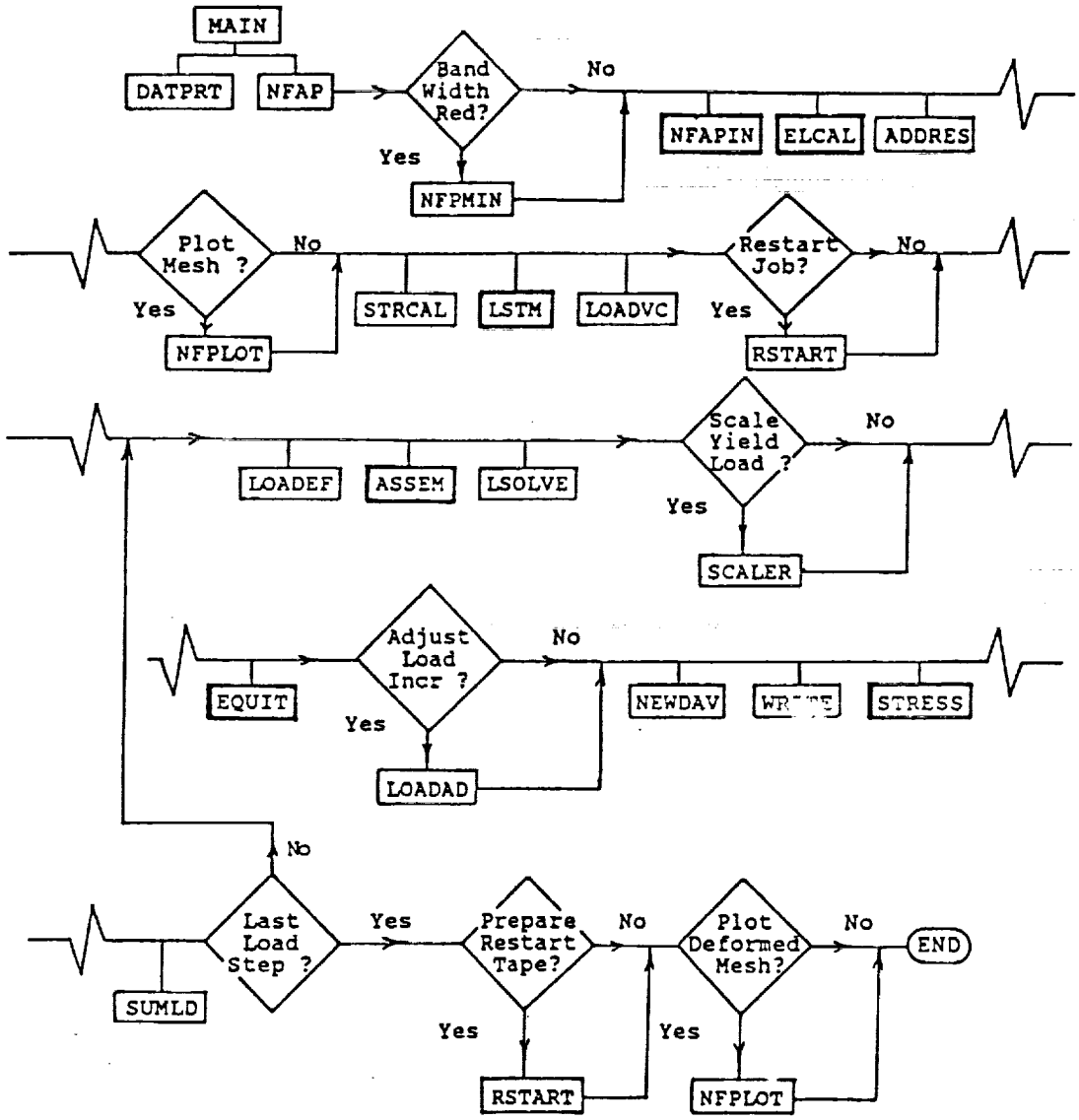

NFAP Program Flow
Figure 6

Figures corresponding to these points of modification are discussed below:

FIGURE 7 : Subroutine NFAPIN processes nodal point data (IND = 0) and directs the pressure load calculations (IND = 2).

FIGURE 8 : ELCAL calls appropriate subroutines to calculate element storage requirements. Any element-related quantities needed at problem start (e.g. nodal connectivity, initial fiber system) are also defined.

FIGURE 9 : LSTM drives the linear analysis. Element stiffness matrices are computed and then stored in ADDBAN.

FIGURE 10 : ASSEM directs element stiffness calculation as well. Indicated flow is for the nonlinear case (IND = 4).

FIGURE 11 : EQUIT drives the solution during equilibrium iteration (ICOUNT = 4) in nonlinear analysis.

FIGURE 12 : Element stress calculation for linear analysis or for nonlinear analysis at end of load step.

In total, 19 subroutines are affected by the above modifications. Some are only slightly altered to accomodate the new elements, but in most instances entirely new

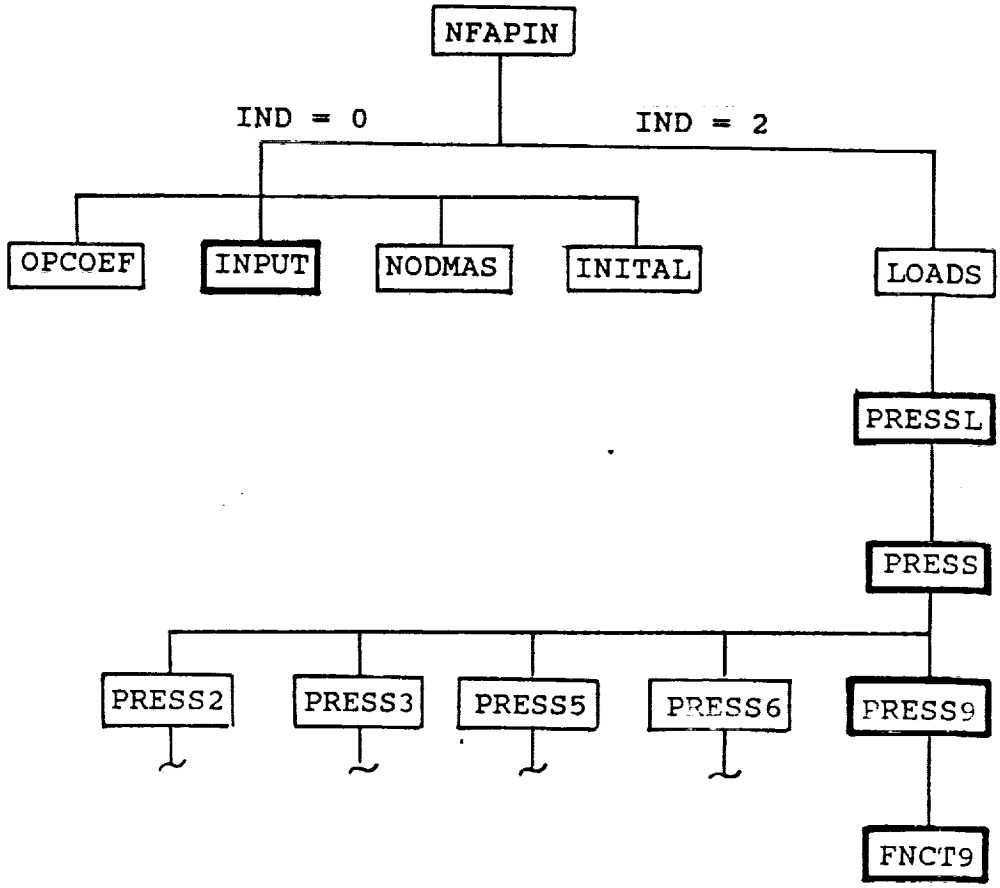

Subroutine NFAPIN
Figure 7

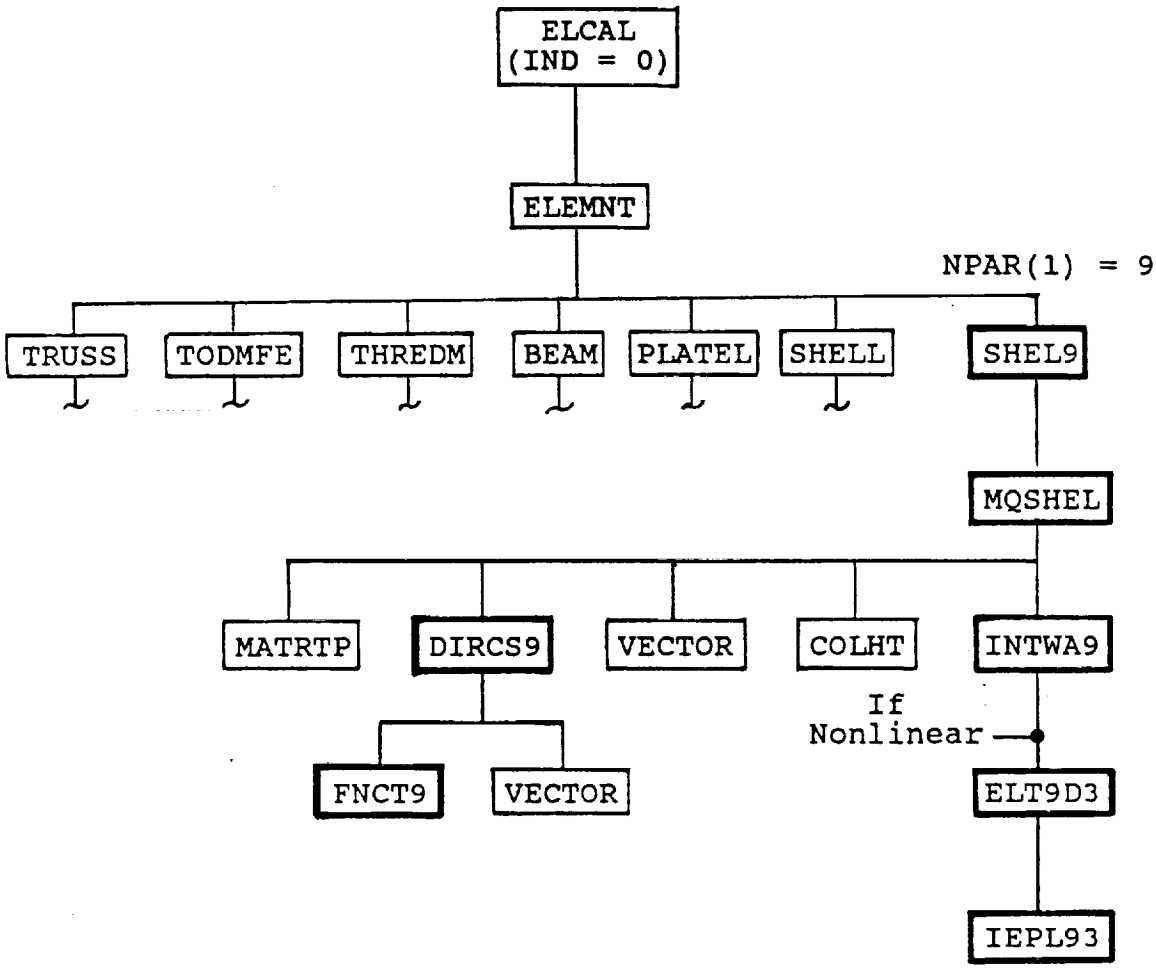

Subroutine ELCAL
Figure 8

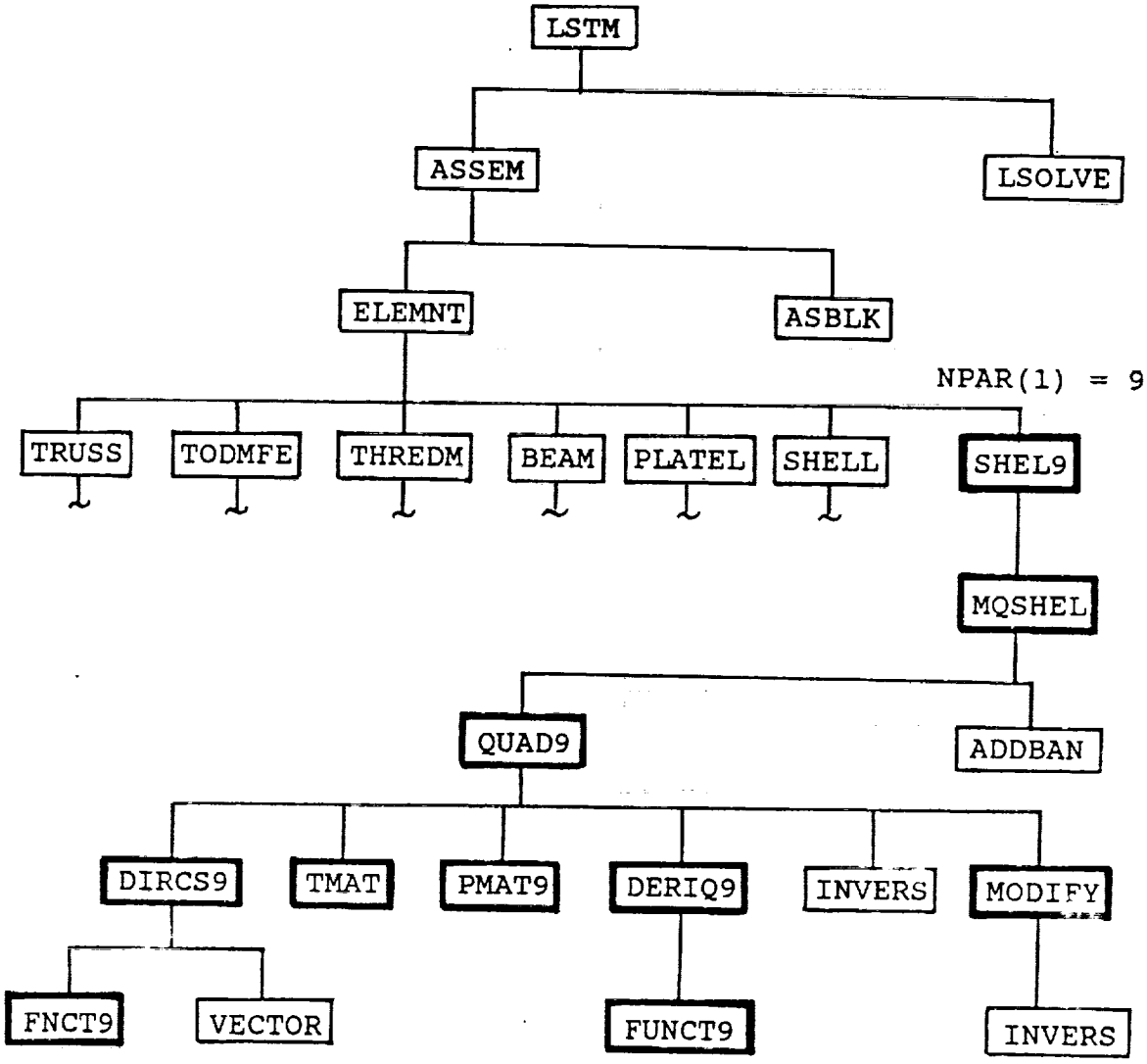

Subroutine LSTM
Figure 9

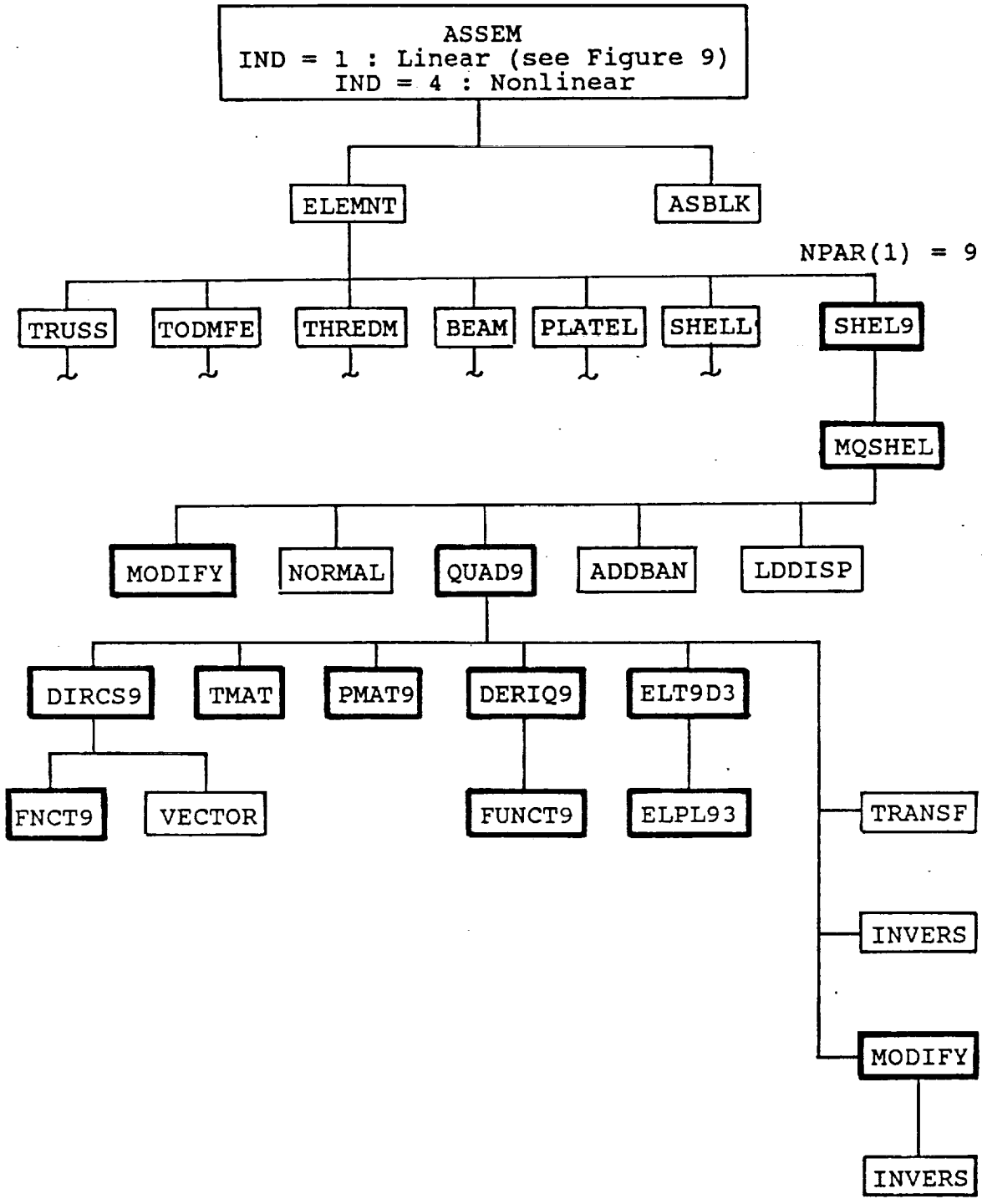

Subroutine ASSEM
Figure 10

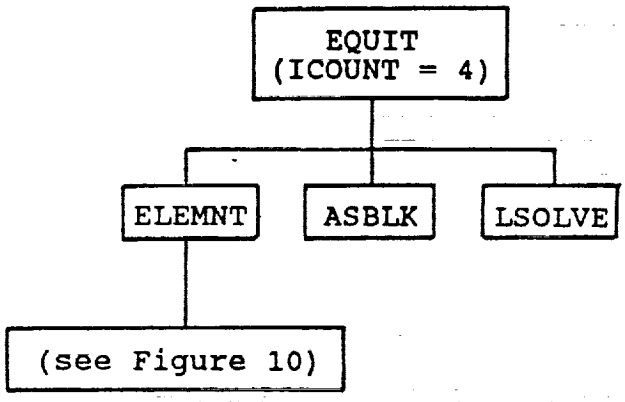

Subroutine EQUIT
Figure 11

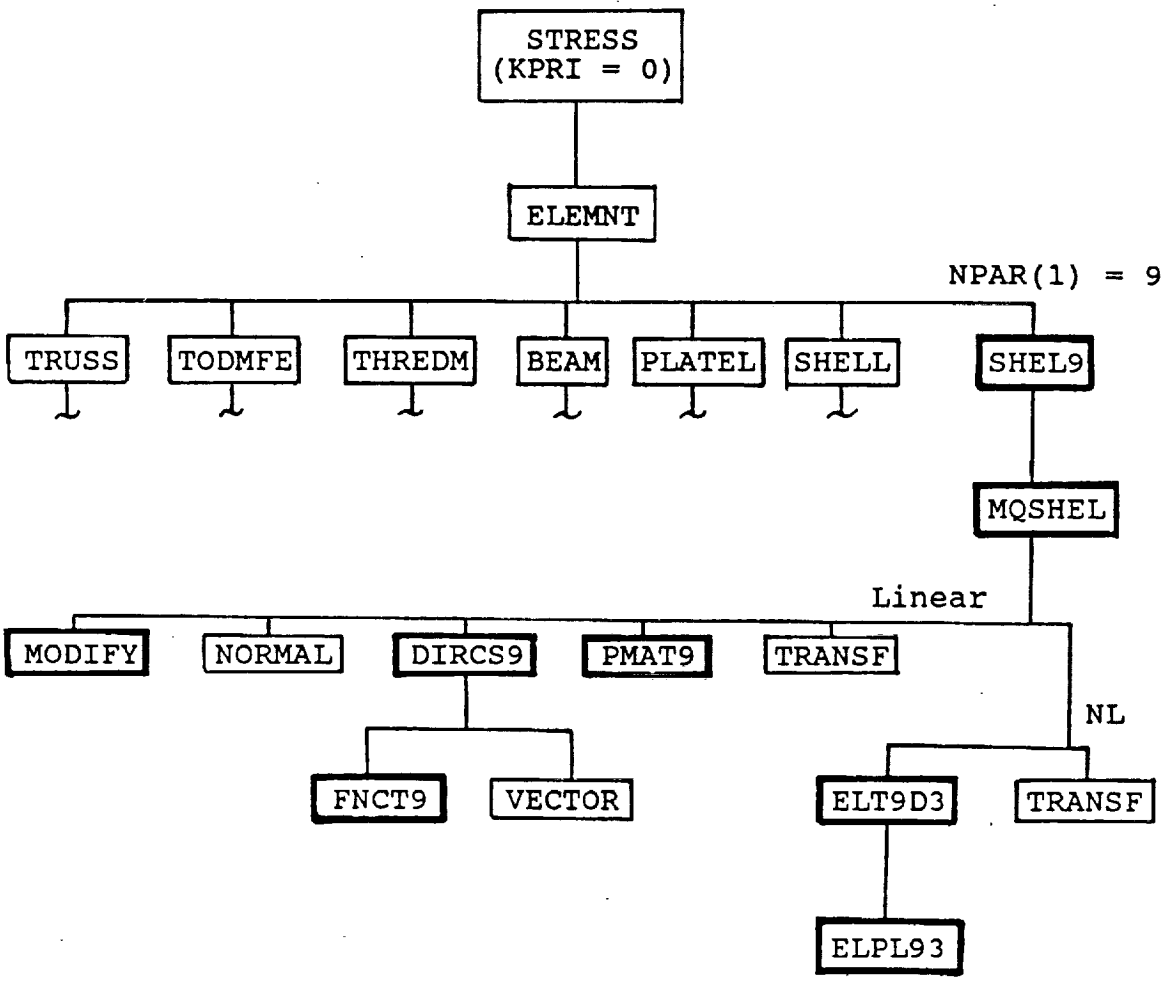

Subroutine STRESS
Figure 12

subroutines (denoted by "*") are written. A description of each follows:

* DERIQ9 : Defines the linear and nonlinear global strain-displacement operators (equations 13 and 14) at integration point (r,s,t).
* DIRCS9 : Driver for construction of the lamina coordinate system (equation 6).
* ELPL93 : Records strain history throughout the nonlinear incremental solution process.
* ELT9D3 : Allocates integration point storage for nonlinear analysis.
* FNCT9 : Calculates shape functions and Jacobian operator at element middle surface.
* FUNCT9 : Calculates shape functions (equation 9) and Jacobian operator at integration point (r,s,t).
* IEPL93 : Initializes storage for the nonlinear problem.

  INPUT : Existing subroutine modified to allow for the two-surface input option (equation 1).
* INTWA9 : Drives storage initialization for nonlinear analysis.
* MODIFY : Calculates condensed stiffness, loads and displacements (equations 56, 58 and 59). Only called if middle node condensation option is active (IETYPE = 1).

* MQSHEL : Driver for the mixed shell element. Defines the fiber system and element nodal connectivity at problem start. Calls appropriate subroutines to calculate and store element stiffness matrices. Directs element stress calculations at the conclusion of each load step.

  NFAPIN : Existing subroutine modified to allow for the two-surface input option (equation 1).

* PMAT9 : Evaluates P-matrix (equations 49-53) at integration point (r,s,t).

  PRESSL : Existing subroutine modified for elements SHELM5 and SHELM9. Drives the pressure load calculations.

  PRESS : Existing subroutine modified for elements SHELM5 and SHELM9. Positions equivalent nodal force pressure loads in global array.

* PRESS9 : Calculates equivalent nodal point forces due to pressure load. Limited to loads applied normal to the shell surface (IFC = 5) and those independent of deformation (IPGD = 0).

* QUAD9 : Drives formation of the element stiffness matrix (equations 26-35 and 38-40).

* SHEL9 : Allocates storage for mixed shell element.

* TMAT : Handles transformation from global to lamina reference frame (equation 7).

As mentioned previously, the current research is confined to geometric nonlinear analysis with small strain. Consequently, when total assumed strains are required ($\underline{e}$ of equations 29 and 31), ELPL93 sums the accumulated incremental strains directly. The corresponding total stress is then obtained according to (43). For large strain analysis, additional transformations would be required. In the present context, these transformations reduce (approximately) to identity matrices.

It is recognized that mixed formulations, when compared to the standard displacement-based models, typically require more CPU time to form element stiffness matrices of the same size. Therefore, any characteristic of the formulation which lends itself to improving the element's efficiency is to be taken full advantage of. As an example, in linear analysis, stress is computed in MQSHEL according to (43*). Rather than re-computing $\underline{H}^{-1}$ and $\underline{G}$, a more efficient strategy would be to write the matrix product to tape as the element stiffness is being formed in QUAD9, and recovering during the stress calculation phase. A similar strategy is invoked for the nonlinear analysis. Not only are $\underline{H}^{-1}$ and $\underline{G}$ written to tape, but comparison of (36) and (40) reveals that the matrix product $\underline{H}^{-1}(\underline{Z}-\underline{W})$ is common to both equations. Therefore, as the right-hand-side load vector term $\underline{Q}_{-2}$ is being constructed in QUAD9 during

iteration "i", the matrix product $\underset{\sim}{H}^{-1}(\underset{\sim}{Z}-\underset{\sim}{W})$ is saved for the incremental strain calculations of iteration "i+1".

6.2 Added Features

The difficulties encountered when attempting to define unique fiber systems at shell interfaces has prompted addition of a two-surface input option. As previously described, this deficiency is artificially embedded in the SHELM5 element for all but the flat plate problems. Since the rotational degrees-of-freedom generated from these fiber coordinates are retained as unknowns in the global system of equations, unique fiber directions are essential if meaningful results are to be obtained.

A second added feature involves a procedure for internally condensing out the SHELM5 center node degrees-of-freedom. Condensation does not in any way enhance the element's analysis capabilities. Instead, it is viewed as more of a cosmetic improvement, since most pre-and-post-processors are not structured to handle elements such as SHELM5.

For SHELM5, interelement continuity requirements concern only the corner nodes, so that center node degrees-of-freedom may be eliminated. In partitioned form, the element equations are written as

$$\begin{bmatrix} \underline{K}_{uu} & \underline{K}_{u\lambda} \\ \underline{K}_{\lambda u} & \underline{K}_{\lambda\lambda} \end{bmatrix} * \begin{bmatrix} \Delta\underline{u} \\ \Delta\underline{\lambda} \end{bmatrix} = \begin{bmatrix} \Delta\underline{R}_u \\ \Delta\underline{R}_\lambda \end{bmatrix} \tag{55}$$

where subscripts "u" and "λ" correspond to the retained corner node and condensed central node degrees-of-freedom, respectively. Incremental central node displacements are obtained from (55) as

$$\Delta\underline{\lambda} = \underline{K}_{\lambda\lambda}^{-1} [\, \Delta\underline{R}_\lambda - \underline{K}_{u\lambda}^{T} \Delta\underline{u} \,] \tag{56}$$

Substitution of (56) back into the first of equations (55) leads to

$$\overline{\underline{K}} * \Delta\underline{u} = \Delta\overline{\underline{R}} \tag{57}$$

where,

$$\begin{aligned} \overline{\underline{K}} &= \text{condensed element stiffness} \\ &= \underline{K}_{uu} - \underline{K}_{u\lambda} \underline{K}_{\lambda\lambda}^{-1} \underline{K}_{\lambda u} \end{aligned} \tag{58}$$

$$\begin{aligned} \Delta\overline{\underline{R}} &= \text{condensed incremental load vector} \\ &= \Delta\underline{R}_u - \underline{K}_{u\lambda} \underline{K}_{\lambda\lambda}^{-1} \Delta\underline{R}_\lambda \end{aligned} \tag{59}$$

Since the order of the system matrices has been lowered, storage requirements are likewise reduced.

6.3 Help for the New User

Although it is not necessary for the user to possess knowledge of the formulation's underlying theory, he/she must still be aware of potential problem areas. As has been repeatedly stated, knowing the conditions under which

equation (2) may be correctly used to define the fiber direction is fundamental to obtaining meaningful results. The user must also be familiar with the method in which rotational degrees-of-freedom are defined internally (equations 3 and 4) in order to accurately specify boundary conditions on rotations. The above considerations are common to many middle surface shell element formulations and should not be interpreted as a deficiency unique to the present work.

As described earlier, SHELM5 and SHELM9 were developed for small strain, geometric nonlinear analysis only. Additional items which the user should be aware of are given in Chapter 7.

CHAPTER 7

NUMERICAL RESULTS

As outlined in Chapter 6, elements SHELM5 and SHELM9 have been implemented into NFAP [17], a general-purpose nonlinear finite element program. All calculations reported herein were performed in double-precision on the IBM 3033 Computer at the University of Akron.

The linear problem set (Sections 7.1-7.3) is simply a collection of some of the more dramatic results presented in previous papers [19,61]. Those additional problems comprising the nonlinear set (Sections 7.4-7.11) are of course restricted to small strain, geometric nonlinear analysis. Other considerations/limitations include:

* Integration order: for both linear and nonlinear analysis, a (3x3x2) scheme is recommended
* Convergence criteria: displacement-controlled, where the incremental norm must be less than 1/1000 of the norm of total displacements

$$|| \Delta \underline{u} || < 0.001 * || \underline{u} ||$$

* Solution method: all full Newton-Raphson (FNR), i.e. stiffness reformed for every iteration of each load step
* Formulation type: an UL approach is used exclusively
* Analysis type: static, i.e. no dynamic or frequency analysis capabilities presently exist
* Pressure loading: must be independent of deformation (IPGD = 0), with loads permitted on the shell surface only (IFC = 5)

Load step and solution time information for the nonlinear problem set is provided in Appendices A and B, respectively.

For discussion purposes, the various elements used for comparison in the numerical results to follow are designated as

Q9 : 9-node isoparametric displacement-based element with exact integration

Q9-URI : 9-node isoparametric displacement-based element with uniform reduced integration

Q9-γ : 9-node isoparametric displacement-based element with uniform reduced integration and stabilization matrix [10]

7.1 Patch Test

An important convergence requirement for an element is to pass the patch test for arbitrary geometry. A mesh of distorted elements are subjected to a loading which, in an exact analysis, corresponds to constant strain conditions. If the element does in fact represent the constant strain state, the patch test is passed.

In this context, for bending analysis, the element assemblage must be able to assume a state of constant curvature. To investigate element behavior in this regard, a square cantilever plate subject to a line bending moment along the free edge is considered. Mesh configurations are shown in Figure 13 for SHELM9. Results for SHELM5 were generated using similar (4x4) mesh layouts. As displayed in Table 1, both elements are relatively insensitive to distortions. Exact correlation is not to be expected, since the transformation defined by (54) is only a constant-value averaged correction.

7.2 Morley's Thin Rhombic Plate

Skew plates have in the past been a particularly challenging problem due to the singular nature of bending moments at obtuse corners [45]. Additionally, since arbitrary distortions can be compensative, unidirectionally skewed mesh patterns may in fact be the more severe test of nonrectangular element performance.

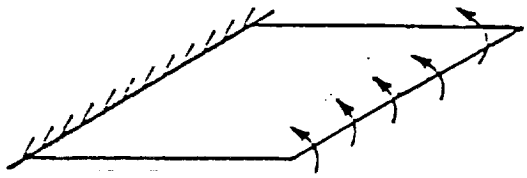

Moment = 0.50
Length = 10 (square)
Thickness = 0.10
E = 30,000
ν = 0.30

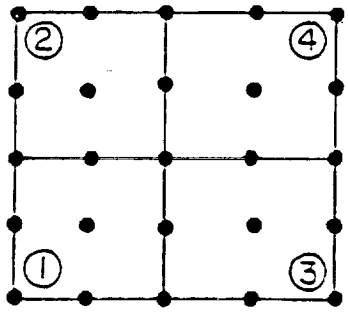

(a) Regular

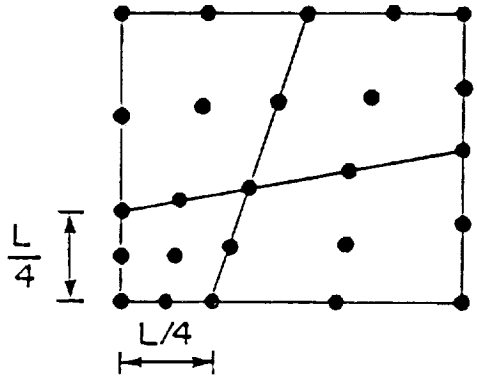

(b) Linear Distortion

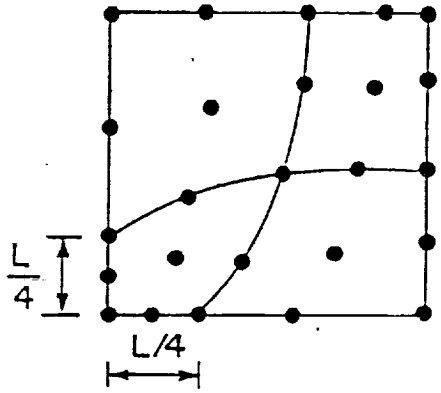

(c) Curved Distortion

Patch Test Mesh Configurations
Figure 13

Table 1

Patch Test Deflections and Stresses

	Normalized Deflection	Normalized Bending Stress @ Element Centroid			
		1	2	3	4
Regular Mesh	1.00	1.00	1.00	1.00	1.00
Linear Distortion	0.99	0.95	1.01	0.98	0.99
Curved Distortion	0.98	0.97	0.98	0.99	0.99

(a) SHELM5

	Normalized Deflection	Normalized Bending Stress @ Element Centroid			
		1	2	3	4
Regular Mesh	1.00	1.00	1.00	1.00	1.00
Linear Distortion	1.00	1.00	1.00	1.00	1.00
Curved Distortion	0.99	1.01	0.99	0.97	0.98

(b) SHELM9

NOTE : Deflections reported are at midpoint of the free edge. For SHELM5, centroidal stresses are for the four extreme corner elements.

With consideration for the above remarks, element behavior when severely distorted is examined by considering the pressure-loaded skew plate of Figure 14. Depicted is the (2x2) mesh configuration (N=5) for SHELM9.

Importance of the planar Jacobian transformation is demonstrated in Table 2. Failing to consider (54) when interpolating strain, results in an artificially stiff response. When the transformation is included, convergence is much improved.

7.3 Truncated Hemispherical Shell

Mesh geometry and other pertinent information are given in Figure 15. Due to symmetry, only one-fourth of the shell is discretized. This is one of a series of recommended benchmark problems designed to determine behavioral characteristics of new shell elements [42]. Loading is such that large sections of the shell rotate almost as rigid bodies, making this a particularly challenging problem. Because this nearly rigid body motion involves little membrane action, the potential for locking is great.

Convergence curves for normalized displacements at point of load application are plotted in Figure 16. Despite being of lower order, SHELM5 converges faster than any of the 9-node elements considered, including SHELM9. The standard displacement-based element with exact integration is a big disappointment. This was almost to be anticipated

Pressure load = 0.001
Length = 100
Thickness = 0.10
E = 445,530
ν = 0.30
α = 30°
All edges simply supported

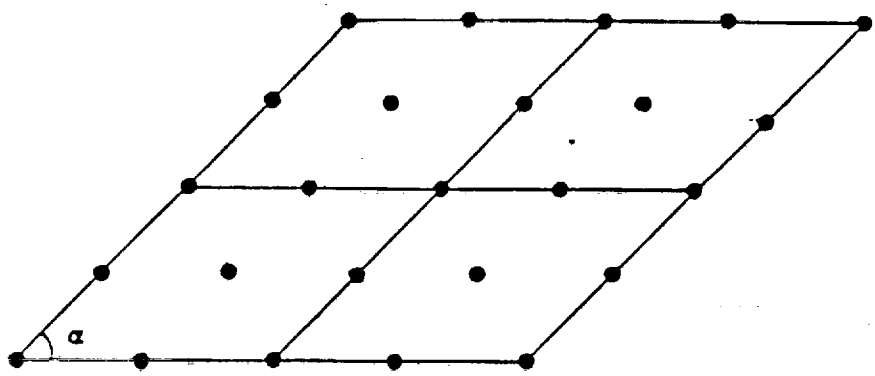

Thin Rhombic Plate
Figure 14

Table 2

Thin Rhombic Plate Deflections and Moments

N	Normalized Maximum Deflection			
	without eqtn. (54)		with eqtn. (54)	
	SHELM5	SHELM9	SHELM5	SHELM9
5	0.691	0.498	0.939	1.046
9	0.721	0.759	0.899	0.920
13		0.815		0.908
17		0.844		0.915
33		0.897		0.946

N	Normalized Maximum Moment			
	without eqtn. (54)		with eqtn. (54)	
	SHELM5	SHELM9	SHELM5	SHELM9
5	0.565	0.548	0.848	1.088
9	0.647	0.842	0.906	0.938
13		0.873		0.937
17		0.897		0.947
33		0.935		0.967

NOTE : N is the number of nodes along plate edge

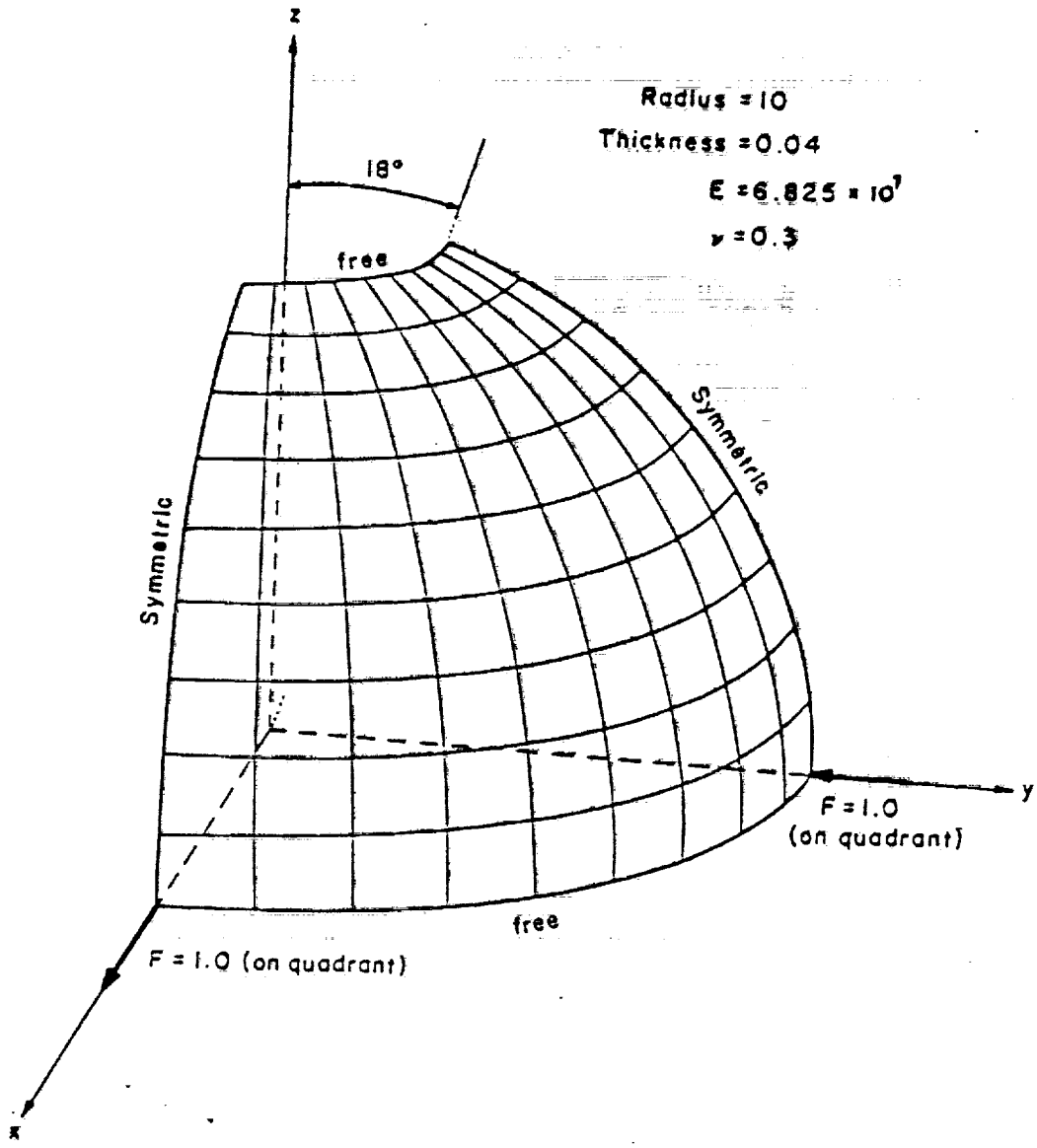

Truncated Hemispherical Shell
Figure 15

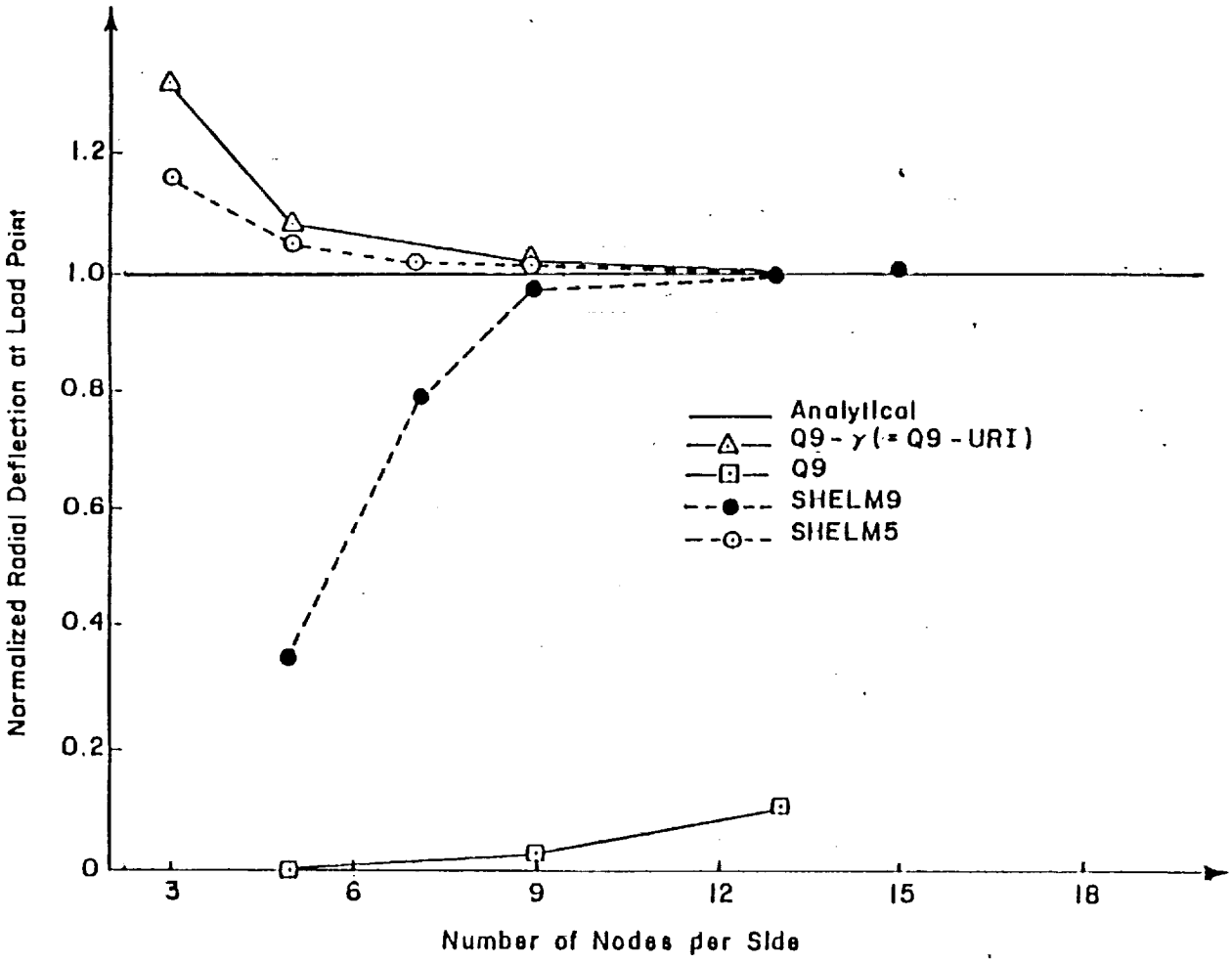

Displacement Convergence for the Truncated Hemispherical Shell
Figure 16

though, considering the severity of the problem. As an aside, non-detrimental effects of the stabilization matrix are noted, as Q9-Y and Q9-URI yield identical results.

7.4 Cantilever Beam with End Moment

A moment-loaded cantilever beam was selected to begin the nonlinear study. Because of its simplicity (essentially 2D with no shear/membrane locking concerns) and the availability of an analytical solution, this problem is particularly well-suited for initial verification of geometric nonlinear portions of the code.

Structure geometry and normalized displacements as a function of loading are illustrated in Figure 17. For clarity, SHELM9 has been omitted, as its response is almost identical to that of SHELM5 and Q9-URI. Even though large nonlinear deformations were involved, none of the elements considered experienced convergence difficulties. This is not surprising, in light of the relatively unconstrained nature of the problem.

Also of note is that the mixed elements required essentially the same number of iterations over the full loading history as Q9-URI (see Appendix B). As discussed in Section 2.3, a lesser number was expected. Again, this might also be attributed to the problem simplicity.

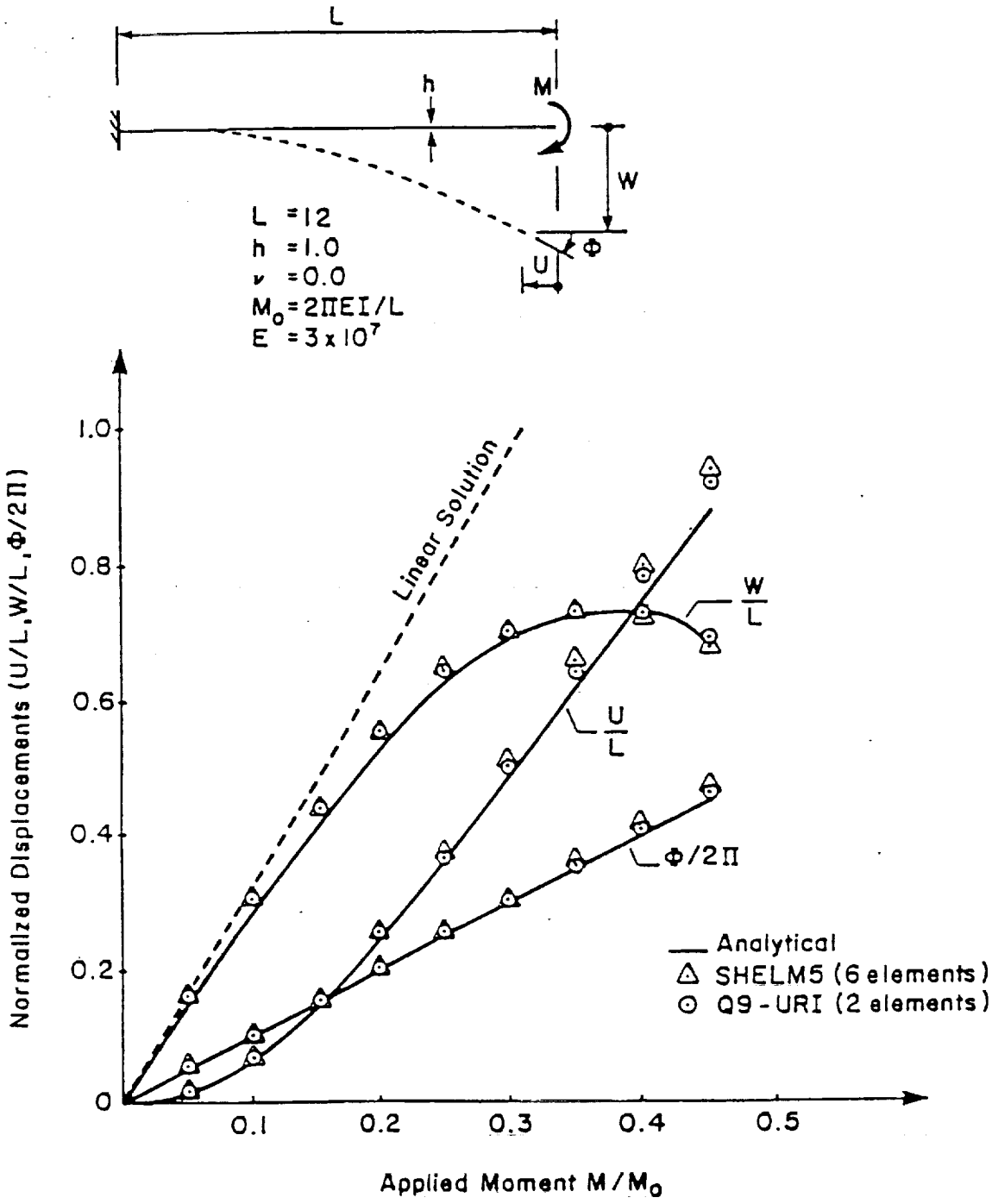

Cantilever Beam with End Moment
Figure 17

7.5 Cantilever Beam with End Shear

This is a somewhat more challenging problem than the one just considered. Here, the beam is thin (L/h = 100) and subject to transverse shear, so that locking is now a point of concern.

Figure 18 illustrates the structure geometry along with a plot of displacements as a function of load. Again, SHELM9 has been omitted for clarity. Although deformations again were rather large (U/L = 0.32, W/L = 0.67), no problems were encountered. Because the mixed elements now converge in fewer total iterations, the CPU time ratio has been reduced (compare Sections 7.4 and 7.5 in Appendix B).

7.6 Shallow Shell Subject to Concentrated Load

The level of complexity is raised another notch, as membrane forces are now responsible for carrying a portion of the load. If the shell is shallow however, there is only a mild coupling of bending and membrane actions. Consequently, accurate representation of shallow shells typically is well within the capabilities of most shell elements.

Information pertinent to this problem is given in Figure 19. Because of symmetry, only one-quarter of the shell is considered in the finite element discretization. Once more, for clarity the SHELM9 plot is omitted, with only the snap-through load level reported. Again, each of the elements considered were trouble-free.

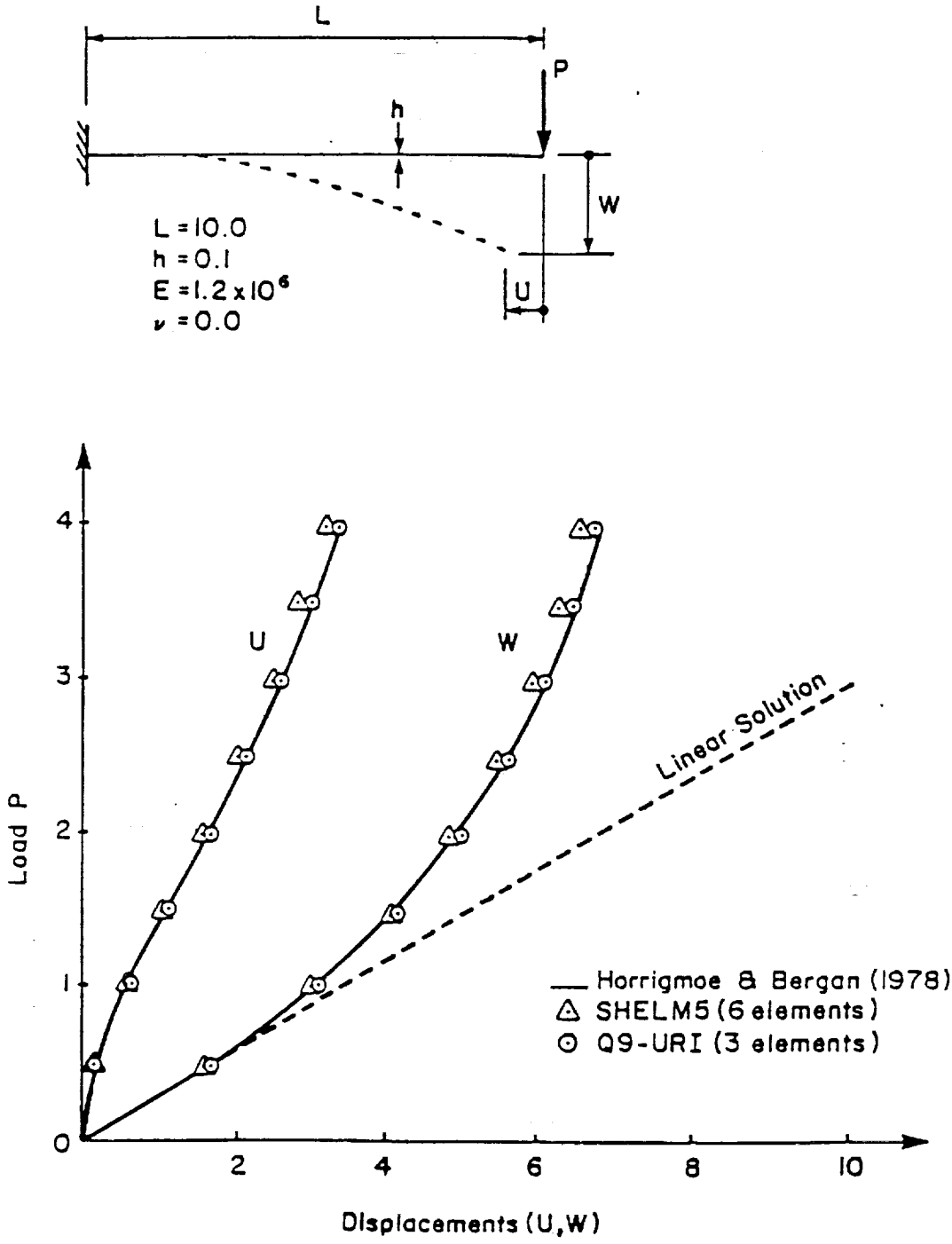

Cantilever Beam with End Shear
Figure 18

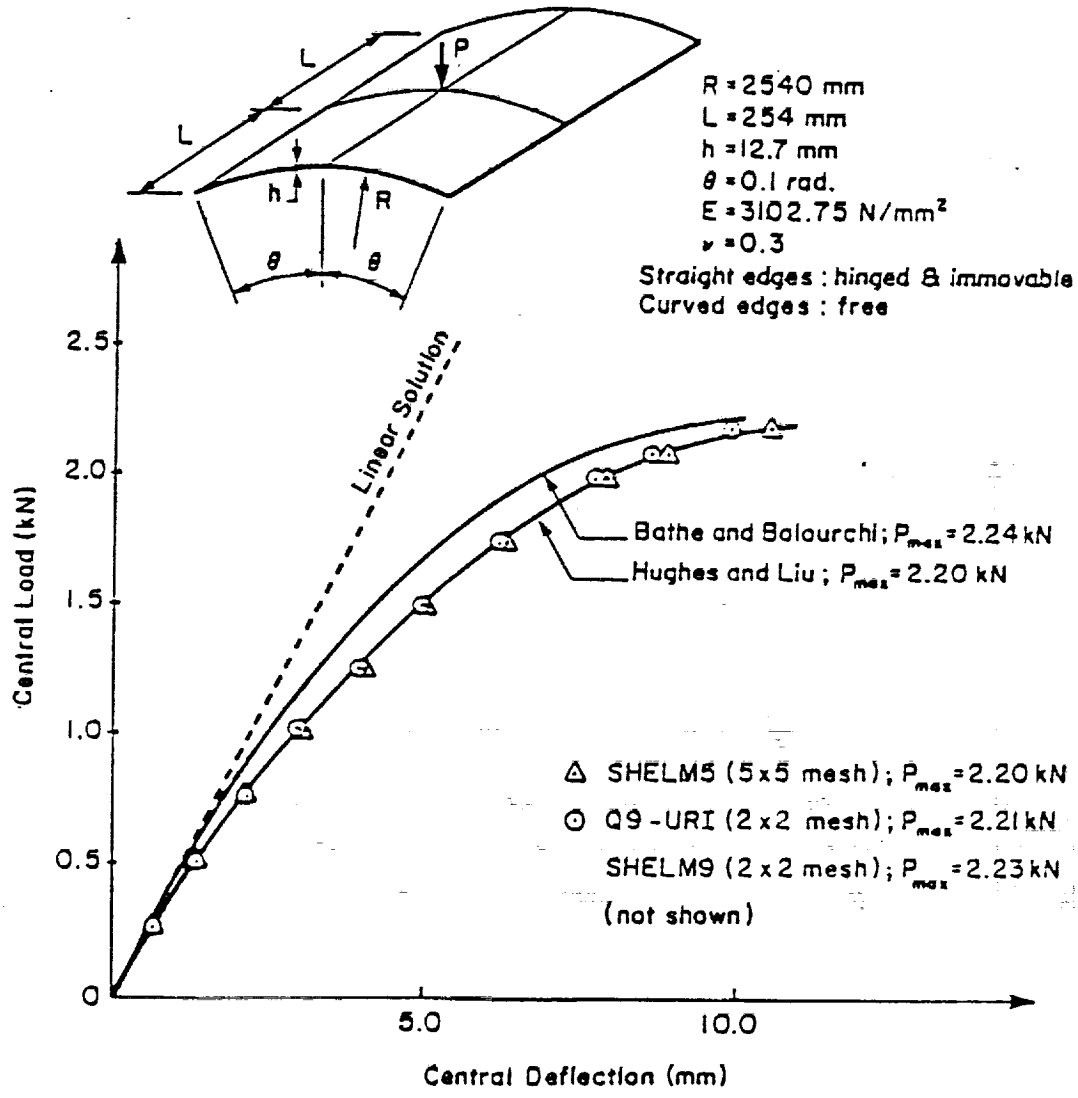

Shallow Shell Subject to Concentrated Load
Figure 19

Though difficult to determine quantitatively just how many added membrane constraints are introduced, because of the shell's shallowness, additional constraints should be of secondary importance. In this particular case, boundary restraints (immovable supports along the straight edges) are such that a substantial portion of the strain energy will be membranal. As a result, inextensional bending modes are not crucial and membrane locking should not be a major concern here.

7.7 Pinched Cylindrical Shell

Element behavior for deep shell geometric nonlinear analysis is now investigated. Structure geometry, loading, boundary conditions and material properties are given in Figure 20. Again, symmetry conditions are such that only one-eighth of the shell need be considered. This is one of the more severe tests available, since complex bending-membrane coupling action (region C) and inextensional modes (regions A, B and D) are both present.

Load-deflection curves are plotted in Figure 21. Though each of the elements remain numerically stable, we now begin to see small deviations in reported results. In the absence of an analytical solution, no further comments in regard to element accuracy are made. Here again, given the same mesh and load step sizes, SHELM9 is converging in fewer iterations than Q9-URI, resulting in further reduction of the CPU time ratio (see Appendix B).

Data:

R = 100
L/R = 2
R/h = 100
E = 3×10^4
ν = 0.3

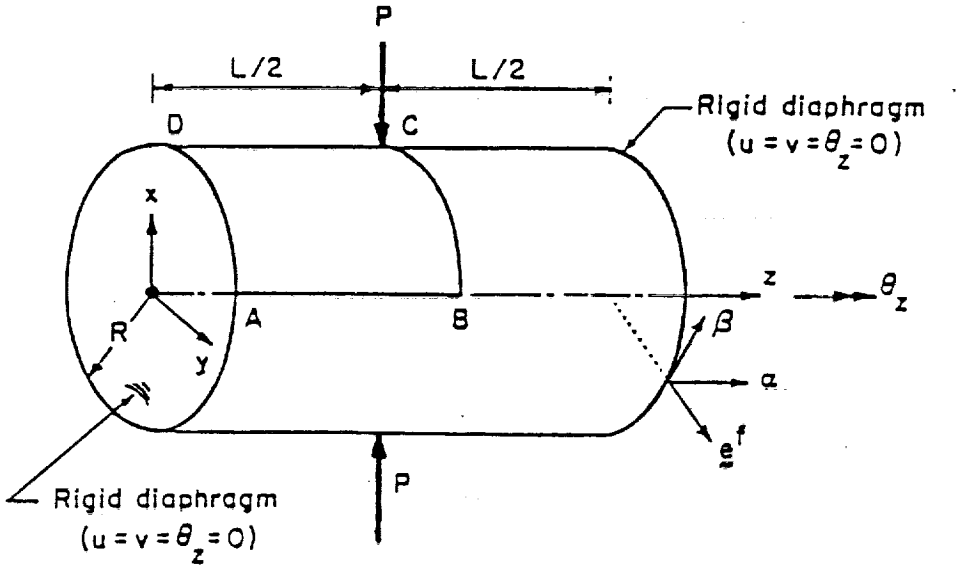

Pinched Cylindrical Shell with End Diaphragms
Figure 20

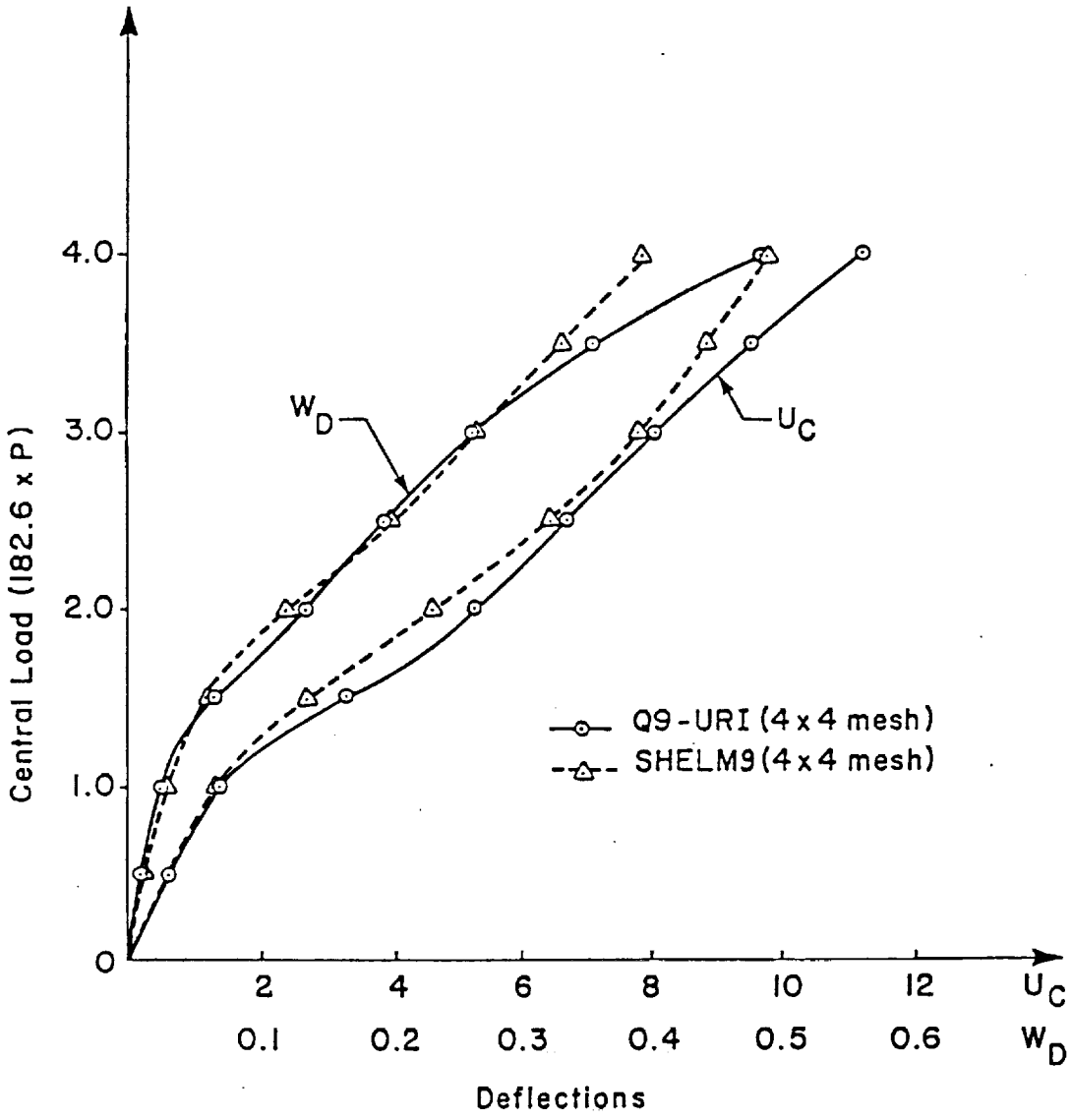

Load-Deflection Curves for Pinched Cylindrical Shell
Figure 21

7.8 Cylindrical Bending of Square Plate Subject to Gravity Load

Due to their highly nonlinear (geometric) response, the cylindrical bending problems of this and the subsequent two sections are particularly severe tests for any shell element. Loading is such that maximum deflections are on the order of 500 times the plate thickness, with rotations on the order of one radian. Since the plate is permitted to "flow" into the cavity when loaded (see Figure 22), in-plane stretching is small and deformations remain elastic. Conditions such as these typically are encountered in the "binder wrap" phase of sheet metal forming operations [20].

Structure geometry and normalized displacements as a function of loading are shown in Figure 22. Indicated mesh sizes are for the one-quarter plate (due to symmetry). The lower order SHELM5 element experienced no difficulties. SHELM9 however, despite having double the number of degrees-of-freedom, is observed to be stiff. Increasing the order of integration from (3x3x2) to (4x4x2) was of no help. Element Q9-URI fared even worse. The displacement-based element failed to converge for even the first load step. Convergence was still a problem when loads were further subdivided into 200 equal steps! Interestingly enough, these same element meshes which were inadequate for the nonlinear problem, yielded exact solutions when used in the corresponding linear analysis.

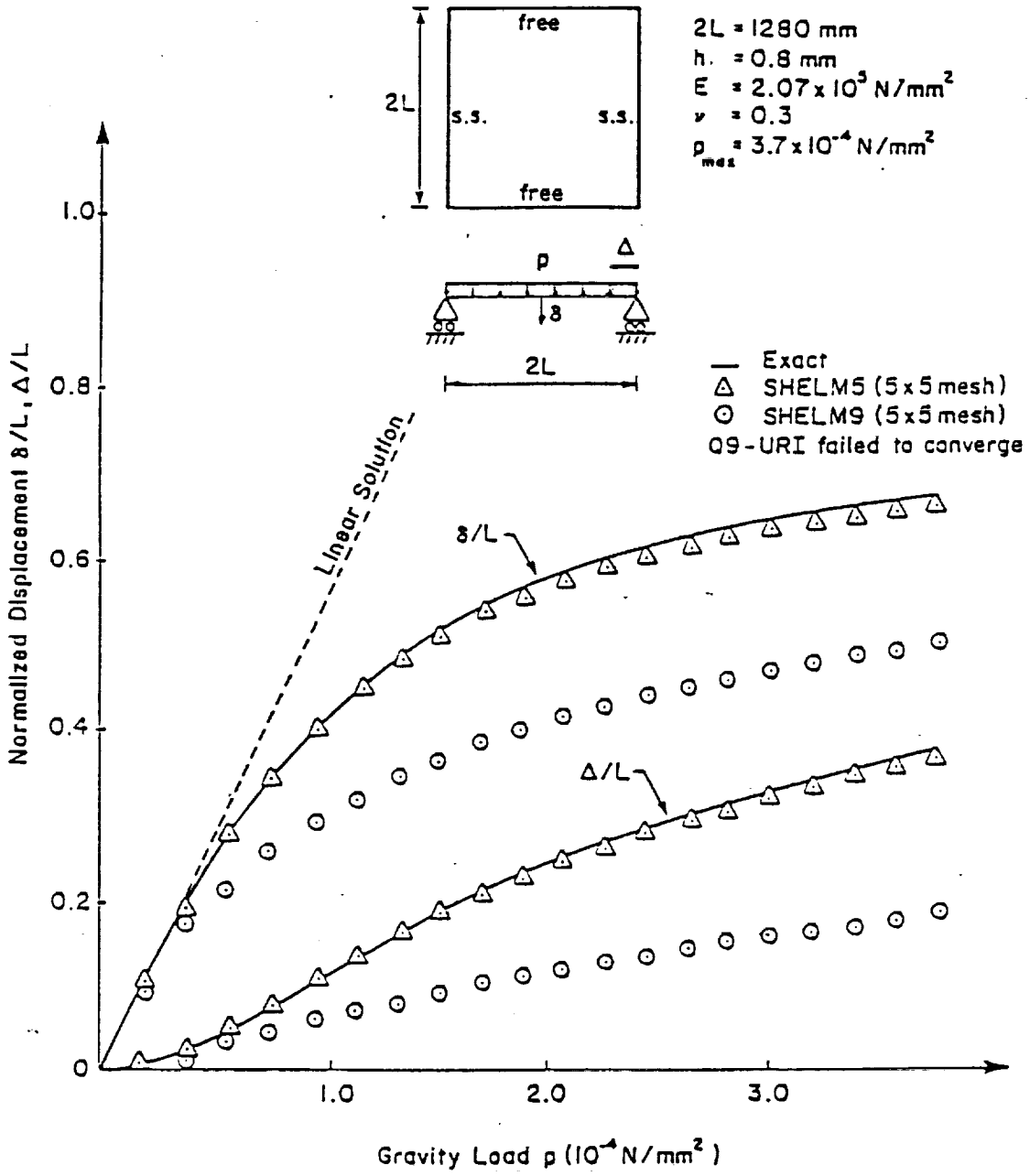

Cylindrical Bending of Square Plate
Subject to Gravity Load
Figure 22

Constraint concepts again provide a means for helping to explain the unusual behavior of elements SHELM9 and Q9-URI described above. Given the plate's thinness (2L/h = 1600) and loading, shear constraints most certainly must be considered. The roller supports limit in-plane stretching so that, once deformation has proceeded far enough for shell action to take over, membrane constraints also become active (note that SHELM9 is still fairly accurate for the first two data points). Finally, since bending occurs in one direction only, additional constraints associated with the off-bending direction are also introduced (three for SHELM5 and six for SHELM9; see equations 49, 51 and 53). The net effect of constraints entering in on three different levels apparently is too much for elements SHELM9 and Q9-URI to handle. What on the surface appeared to be a fairly straightforward nonlinear plate bending problem, has in fact turned out to be a monster!

7.9 Cylindrical Bending of Square Plate Subject to a Line Force

Pertinent information for this test case is given in Figure 23. Except for loading, it is identical to the previous problem. It has been included primarily to facilitate making comparisons with its "beam equivalent" in Section 7.5.

C-2

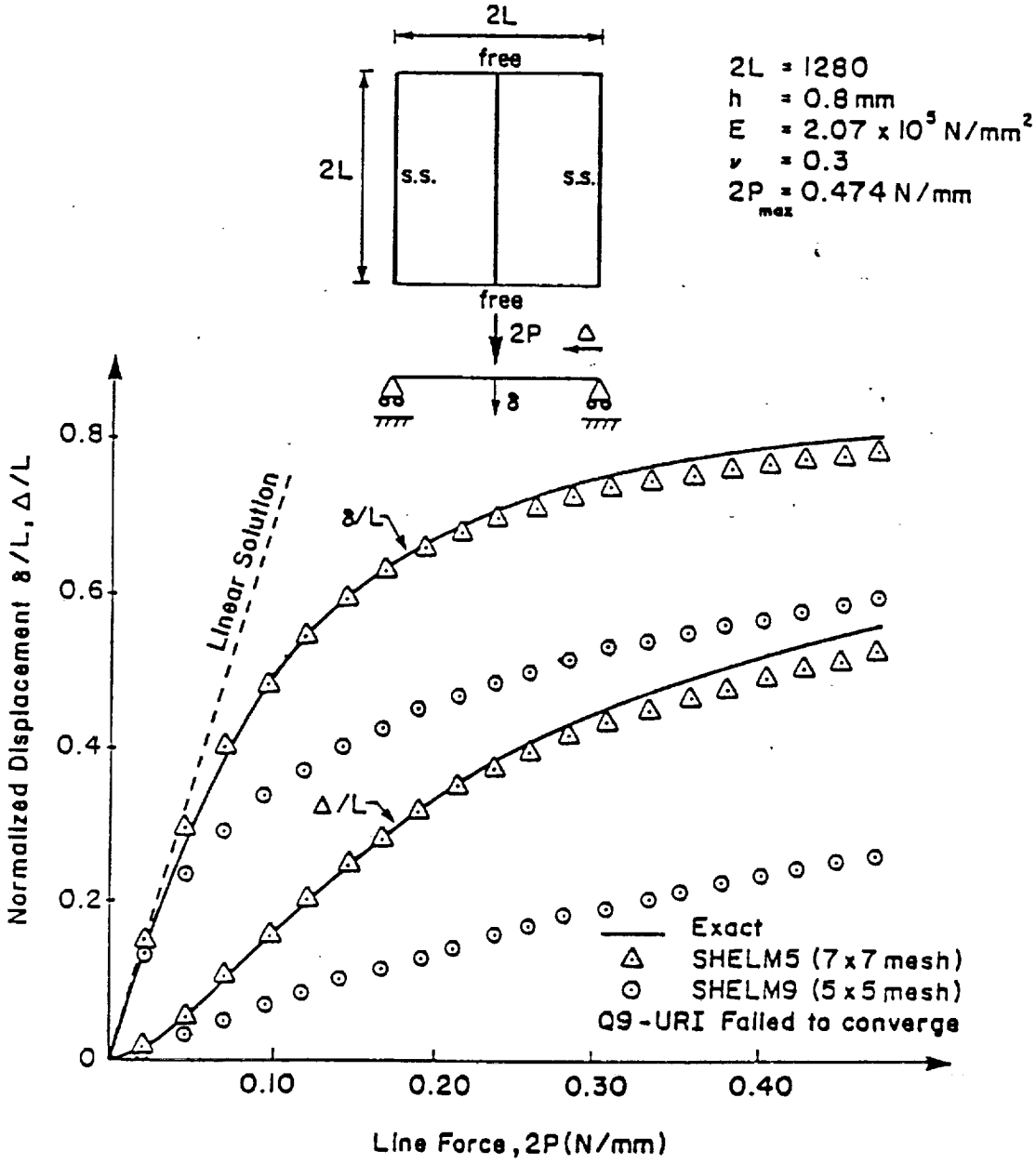

Cylindrical Bending of Square Plate
Subject to Line Force
Figure 23

As in the previous example, SHELM5 experiences no difficulties, while SHELM9 is noticeably stiff and Q9-URI again failed to converge. Of additional interest is that the "beam equivalents" of SHELM9 and Q9-URI in Section 7.5 suffered no similar degradation. There, with the third direction small in comparison to the beam length, off-bending direction constraints are not significant. Also, as before, the corresponding linear analyses yielded the exact solutions.

7.10 Cylindrical Bending of Square Plate Subject to Specified Line Displacements

This example is the conjugate of Problem 7.9, i.e. line displacements rather than line forces are specified along the plate longitudinal axis. It has been included to show the element's capability for analyzing enforced displacement input.

Line forces were calculated from centroidal transverse shear stresses of the element nearest to the plate center. They are plotted as a function of specified displacement in Figure 24. As in the previous two examples, SHELM5 was trouble-free, while SHELM9 and Q9-URI experienced problems.

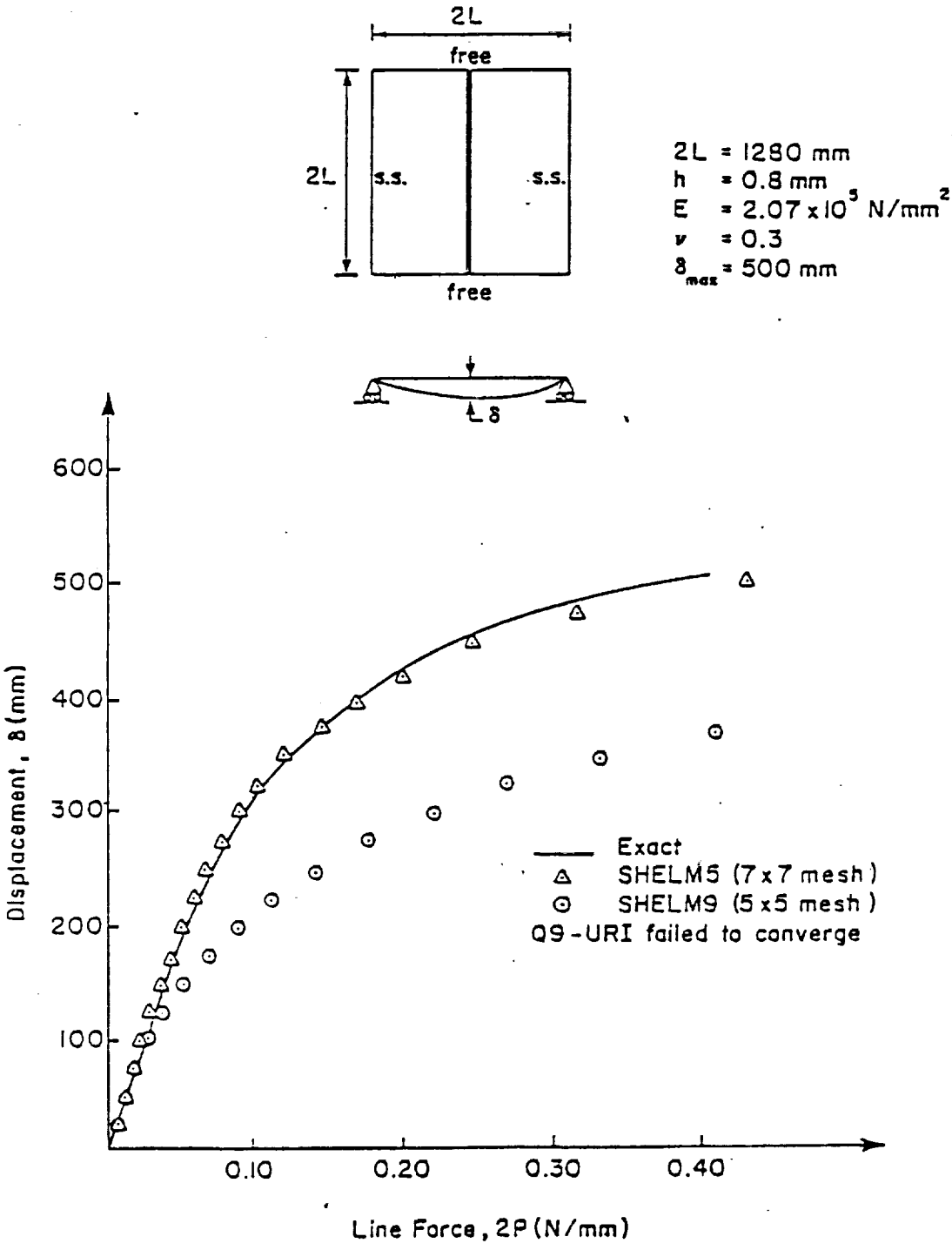

Cylindrical Bending of Square Plate
Subject to Specified Line Displacements
Figure 24

7.11 Simply Supported Square Plate Subject to Gravity Load

This final example is completely analogous to Problem 7.8, except that now all four plate edges are simply supported. Difficulties encountered in the earlier problem were attributed to boundary conditions which activated an unusually high number of in-plane and bending constraints. It is speculated that, by simply supporting all four edges, the structure will now exhibit true biaxial plate bending behavior, thereby relaxing many of these constraints.

Analysis results are presented in Figure 25. Once again, SHELM9's plot has been omitted, as its response is almost identical to that of Q9-URI for the less constrained problem. As postulated, the additional restraint has indeed enabled both SHELM9 and Q9-URI to now obtain accurate, convergent solutions (the latter, only after considerable "searching" to find an appropriate convergent step size).

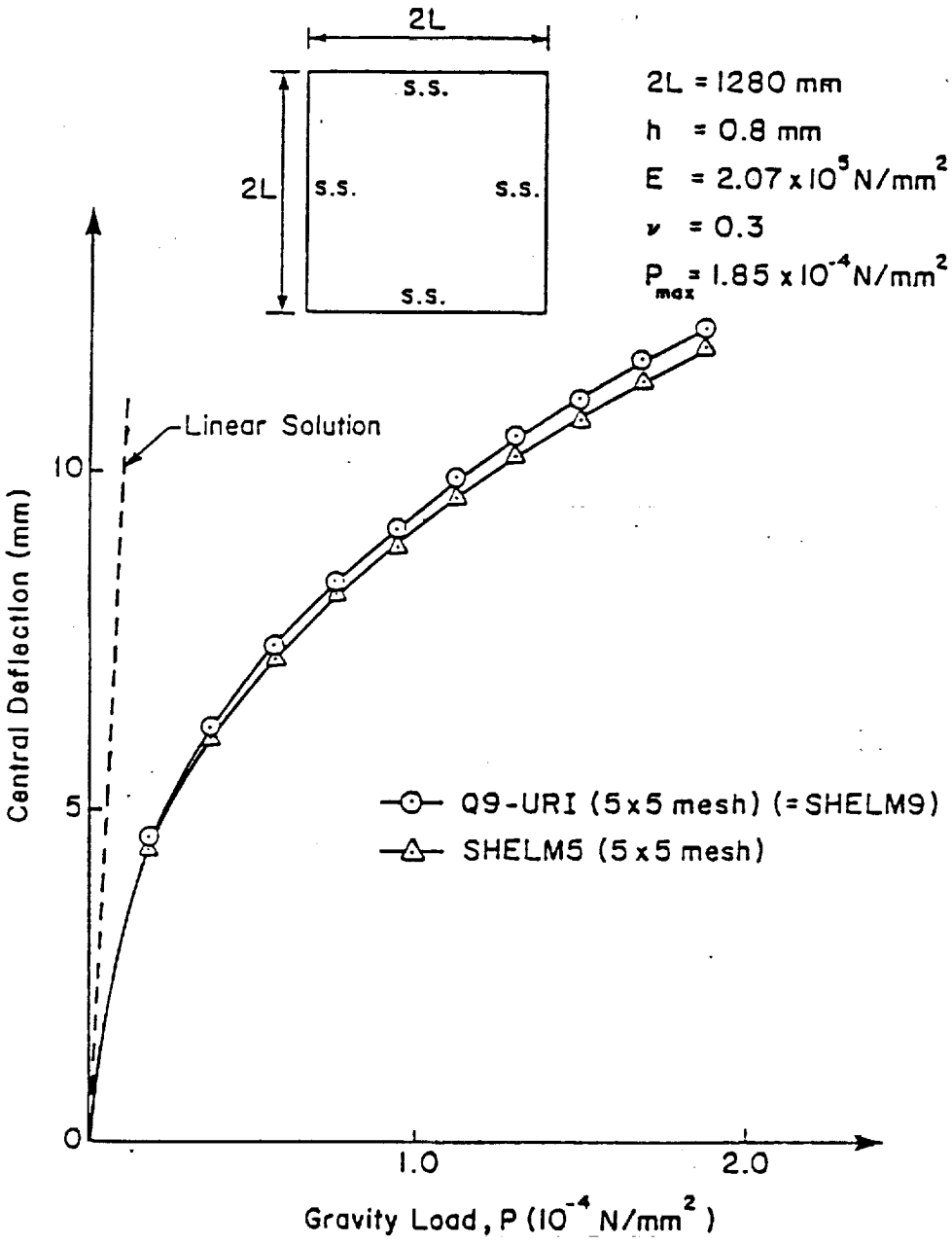

Simply Supported Square Plate Subject to Gravity Load
Figure 25

CHAPTER 8

SUMMARY

8.1 A Brief Review

Numerous methods are presently available to analyze thin plate and shell structures. Assessing the merits and drawbacks of some of the more popular current approaches, a degenerated mixed shell element was chosen for the present study. In particular, it was proposed that the analysis capabilities of the linear 5 and 9-node elements of [61] and [19] be extended to include geometric nonlinearities.

Methodology necessary to effectively track an element's location and subsequent deformation during the iterative step-by-step solution process was described. To that end, extensive reference was made to the concepts set forth in [34] concerning construction of element-level lamina and fiber coordinate systems.

Element development was then traced from the incremental variational principle on through to the final set of equilibrium equations. A procedure for recovering the linear element was also outlined.

Strain parameters were then selected according to a set of guidelines compiled in [19,54,61]. This, in turn, stimulated a discussion regarding constraint index concepts

and their predictive capability related to locking in shells. Special procedures for limiting the element's sensitivity to distortion were also described.

Details of modifications necessary to incorporate the elements into a general-purpose nonlinear finite element program were discussed. Included were descriptions of: (i) a two-surface input option, and (ii) a procedure for internally condensing out center node degrees-of-freedom. Helpful hints and guidelines for the new user were also provided.

Finally, performance characteristics of the elements were evaluated in a wide variety of linear and nonlinear plate/shell problems. Despite being of lower order, the 5-node element proved superior, particularly in severely constrained applications.

8.2 Significant Findings

Despite limiting the research to linear and geometric nonlinear static analysis, a substantial amount of additional insight has been provided concerning the finite element modelling of thin plate/shell structures. Some of this information has also been reported in a parallel but independent research effort at the University of Maryland [58]. The more dramatic discoveries, however, are exclusive to the present work. The reference here is to those insights not confined to mixed formulations, but rather are

relevant to finite element methods in general (see items 7 and 8 to follow).

Significant findings related to this research are listed below. A more detailed discussion of each item then follows.

Concurrently with the University of Maryland

1) More streamlined than previous mixed formulations
2) Necessity of including the strain-displacement mismatch terms in mixed formulations (see also [51])

Exclusive to this Research

3) A numerical study illustrating the need for inclusion of a covariant coordinate transformation for severely skewed elements
4) Necessity of recording strain histories in mixed formulations, even for geometric nonlinear analysis
5) Numerical results to support the claim that, given the same mesh and load step history, mixed elements converge in fewer total iterations than their displacement-based equivalents

6) More evidence provided to support the theory that, in mixed formulations, the lower order elements may be more attractive
7) Numerical results refuting the belief that the same mesh used to obtain accurate linear solutions will necessarily converge to the correct nonlinear solution
8) Discovery of a new form of locking intrinsic to shell elements subjected to uniaxial bending

More subtle contributions include: (i) illustration of yet another constrained media application (see (8) above) where mixed methods prove superior to standard displacement-based formulations, (ii) extending analysis capabilities of SHELM5 and SHELM9 to include geometric nonlinearities, (iii) establishing a procedure for attaching mixed elements to an existing displacement-based finite element program, and (iv) code development for incorporation of two-surface and central node condensation options.

By relaxing the pointwise nonlinear equilibrium requirements and assuming that displacement functions can always be constructed which are compatible across interelement boundaries, the current formulation is much more streamlined than earlier hybrid/mixed methods [16]. The latter condition is easily satisfied for the degenerated shell elements under consideration. As demonstrated in (18), equilibrium is in fact satisfied in an averaged

integral sense, so that the above simplifications are indeed justified.

Since strains are interpolated "independently" from displacements in a mixed formulation, strain-displacement mismatch terms must be retained. These correction terms do not appear in the standard displacement-based element models. There, strains are computed as derivatives of displacements so that, by definition, this relation is automatically satisfied.

Morley's skew plate problem (Section 7.2) demonstrated the need for a covariant coordinate transformation for severely distorted elements. Earlier studies did not consider this effect [58,61].

In displacement-based element formulations, strain is obtained simply by differentiating the total displacement. Mixed formulations, however, interpolate strains incrementally. To determine the total strain, it is therefore necessary to sum and store its history at each integration point throughout the entire solution process.

The iterative solution process involves calculation of out-of-balance right-hand-side load terms, which are directly related to the element's current stress state. Since deformations may be large, elements may also become quite irregular in shape. By evaluating stress more accurately and being less sensitive to distortion, the mixed elements thus typically require fewer total iterations to

converge than equivalent displacement-based elements. Implications of the above are obvious. The entire process of computing, assembling and solving the global system equations is repeated fewer times, resulting in a reduction in computation effort. Thus, the mixed element, despite being more costly insofar as formation of the element stiffness is concerned, is able to recover a portion of this expense in a full-blown, iterative nonlinear analysis.

For the uniaxial bending problem of Sections 7.8-7.10, SHELM5 consistently outperformed SHELM9, despite being of lower order. Apparently the additional degrees-of-freedom gained in moving from a 5 to a 9-node element are offset by an even greater number of added constraints. In this case, the lower order element is preferred.

Sections 7.8-7.10 also served to illustrate that the same mesh which yields an accurate linear response cannot be assured of converging to the correct nonlinear solution. It was theorized in Section 7.8 that this may be a result of shell actions kicking in as deformation proceeds, thereby introducing membrane constraints not present in the linear plate problem. The point to be made is that many research efforts concentrate on the linear formulation, contending that the nonlinear problem is nothing more than a routine extension of the linear development. In light of the data presented, this line of thinking appears questionable (see also [7] for similar observations).

Difficulties associated with shear and membrane locking when modelling thin plate/shell structures are well documented. Other constrained media applications (incompressible materials, contact problems etc.) have also received considerable attention. Another form of locking was encountered in this research (again refer to Sections 7.8-7.10). The shell element, designed for biaxial bending, may not be able to satisfy the additional constraints associated with vanishing of bending strains in the second direction for uniaxial bending.

8.3 Suggestions for Future Work

Having explored only the geometric nonlinear, small strain, static analysis capabilities of elements SHELM5 and SHELM9, many other areas yet remain to be investigated. A second level of research, aimed at improving upon the current development, is also a possibility. Compiled below are some suggestions for future work which address each of these areas. A brief discussion of each item then follows.

1) Improve computational efficiency of present elements using a symbolic manipulator such as MACSYMA [43]
2) Explanation (more quantitative) for the poor behavior of SHELM9 in the test problems of Sections 7.8-7.10

3) Investigation of other constrained media problems
4) Extending element capabilities beyond static, small strain, geometric nonlinear analysis

As indicated in Section 1.1, computational cost considerations have long been a drawback for mixed element formulations. Preliminary results indicate that, for nonlinear applications, closed-form expressions for element stiffness matrices are far too complex. Targeting individual contributions to the stiffness, such as the elastic-plastic material matrix [18], may be more practical. This particular application is of course valid for standard displacement-based formulations as well.

Explaining SHELM9's breakdown in the thin plate uniaxial bending problem may entail a more in-depth study of constraint index concepts. Because of the difficulties associated with interpretation of the constraint index for curved shells, this author has only theorized as to the cause for SHELM9's poor behavior. Since the simply supported version of Problem 7.8 (Problem 7.11) and the "beam equivalent" of Problem 7.9 (Problem 7.5) experience no similar degradation, the constraint index-related explanations provided do, however, appear to have considerable merit.

Whether or not mixed methods find general acceptance in the finite element community in the near future is

debatable. Nevertheless, mixed methods have established themselves in constrained media applications and therefore should be investigated further in this regard. As illustrated in this research, being more costly computationally is not so great of a concern if conventional methods are unable to obtain a solution.

Broadening analysis capabilities of SHELM5 and SHELM9 is also desirable since practical applications are, at present, rather limited. Areas of perhaps greater interest include: (i) large strain analysis, (ii) material nonlinear analysis, (iii) dynamic considerations, (iv) laminated composite analysis, (v) polymer/rubber material modelling, and (vi) high temperature applications.

REFERENCES

[1] Ahmad, S., B.M. Irons and O.C. Zienkiewicz, "Analysis of Thick and Thin Shell Structures by Curved Finite Elements", International Journal for Numerical Methods in Engineering, Volume 2, p. 419-451 (1970).

[2] Argyris, J.H., P.C. Dunne, G.A. Malejannakis and E. Shelke, "A Simple Triangular Facet Shell Element with Applications to Linear and Nonlinear Equilibrium and Elastic Stability Problems", Computer Methods in Applied Mechanics and Engineering, Volume 10, p. 371-403 and Volume 11, p. 97-131 (1977).

[3] Bathe, K.J. and S. Bolourchi, "A Geometric and Material Nonlinear Plate and Shell Element", Computers & Structures, Volume 11, p. 23-48 (1980).

[4] Bathe, K.J., Finite Element Procedures in Engineering Analysis, Prentice-Hall, Englewood Cliffs, NJ (1982).

[5] Bathe, K.J., E.N. Dvorkin and L.W. Ho, "Our Discrete Kirchhoff and Isoparametric Shell Elements for Nonlinear Analysis - An Assessment", Computers & Structures, Volume 16, p. 89-98 (1983).

[6] Bathe, K.J. and E.N. Dvorkin, "A Four-Node Plate Bending Element Based on Mindlin/Reissner Plate Theory and a Mixed Interpolation", International Journal for Numerical Methods in Engineering, Volume 21, p. 367-383 (1985).

[7] Bathe, K.J. and E.N. Dvorkin, "A Formulation of General Shell Elements - The Use of Mixed Interpolation of Tensorial Components", International Journal for Numerical Methods in Engineering, Volume 22, p. 697-722 (1986).

[8] Batoz, J.L., K.J. Bathe and L.W. Ho, "A Study of Three-Node Triangular Plate Bending Elements", International Journal for Numerical Methods in Engineering, Volume 15, p. 1771-1812 (1980).

[9] Batoz, J.L. and M.B. Tahar, "Evaluation of a New Quadrilateral Thin Plate Bending Element", International Journal for Numerical Methods in Engineering, Volume 18, 1655-1677 (1982).

[10] Belytschko, T., C.S. Tsay and W.K. Liu, "A Stabilization Matrix for the Bilinear Mindlin Plate Element", Computer Methods in Applied Mechanics and Engineering, Volume 29, p. 313-327 (1981).

[11] Belytschko, T., W.K. Liu and J.S.J. Ong, "A Consistent Control of Spurious Singular Modes in the 9-Node Lagrange Element for the Laplace and Mindlin Plate Equations", Computer Methods in Applied Mechanics and Engineering, Volume 44, p. 269-295 (1984).

[12] Belytschko, T., H. Stolarski and J. Carpenter, "A C^{o} - Triangular Plate Element with One-Point Quadrature", International Journal for Numerical Methods in Engineering, Volume 20, p. 787-802 (1984).

[13] Belytschko, T., W.K. Liu, J.S.J. Ong and D. Lam, "Implementation and Application of a 9-node Lagrange Shell Element with Spurious Mode Control", Computers & Structures, Volume 20, p. 121-128 (1985).

[14] Belytschko, T., H. Stolarski, W.K. Liu, N. Carpenter and J.S.J. Ong, "Stress Projection for Membrane and Shear Locking in Shell Finite Elements", Computer Methods in Applied Mechanics and Engineering (to appear).

[15] Morgan, P.G. and X. Wang, "Quadrilateral Plate Bending Elements with Shear Deformations", Computers & Structures, Volume 19, p. 25-34 (1984).

[16] Boland, P.L. and T.H.H. Pian, "Large Deflection Analysis of Thin Elastic Structures by the Assumed Stress Hybrid Finite Element Method", Computers & Structures, Volume 7, p. 1-12 (1977).

[17] Chang, T.Y., and S. Prachuktam, "NFAP - A Nonlinear Finite Element Analysis Program", Report No. SE76-3, The University of Akron, Akron, Ohio (1976).

[18] Chang, T.Y., A.F. Saleeb, P.S. Wang and H.Q. Tan, "On the Symbolic Manipulation and Code Generation for Elasto-Plastic Material Matrices", E. neering with Computers, Volume 1, p. 205-215 (1986).

[19] Chang, T.Y., A.F. Saleeb and W. Graf, "On the Mixed Formulation of a 9-Node Lagrange Shell Element", Computer Methods in Applied Mechanics and Engineering (to appear).

[20] Chen, K.K., "Evaluation of a Finite Element for Binder Wrap Calculations", General Motors Research Publication GMR-5209 (1985).

[21] Cook, R.D., Concepts and Applications of Finite Element Analysis, 2nd ed., John Wiley & Sons, New York (1981).

[22] Crisfield, M.A., "A Four-Noded Thin-Plate Bending Element Using Shear Constraint - A Modified Version of Lyons' Element", Computer Methods in Applied Mechanics and Engineering, Volume 38, p. 93-120 (1983).

[23] Dhatt, G., L. Marcotte and Y. Matte, "A New Triangular Discrete Kirchhoff Plate/Shell Element", International Journal for Numerical Methods in Engineering, Volume 23, p. 453-470 (1986).

[24] Dvorkin, E.N. and K.J. Bathe, "A Continuum Mechanics Based Four-Node Shell Element for General Nonlinear Analysis", in Engineering Computations, Pineridge Press, Swansea, Volume 1, p. 77-88 (1984).

[25] Gallagher, R.H., Finite Element Analysis Fundamentals, Prentice-Hall, Englewood Cliffs, NJ (1975).

[26] Graf, W., T.Y. Chang and A.F. Saleeb, "On the Numerical Performance of Three-Dimensional Thick Shell Elements Using a Hybrid/Mixed Formulation", Finite Elements in Analysis and Design, Volume 2, p. 357-375 (1986).

[27] Hinton, E., E.M. Salonen and N. Bicanic, "A Study in Locking Phenomena in Isoparametric Elements", Third MAFELAP Conference, Brunel University, Uxbridge (1978).

[28] Horrigmoe, G. and P.G. Bergan, "Nonlinear Analysis of Free Form Shells by Flat Finite Elements", Computer Methods in Applied Mechanics and Engineering, Volume 16, p. 11-35 (1978).

[29] Huang, H.C. and E. Hinton, "A New Nine Node Degenerated Shell Element with Enhanced Membrane and Shear Interpolation", International Journal for Numerical Methods in Engineering, Volume 22, p. 73-92 (1986).

[30] Hughes, T.J.R., R.L. Taylor and W. Kanoknukulchai, "A Simple and Efficient Finite Element for Plate Bending", International Journal for Numerical Methods in Engineering, Volume 11, p. 1529-1543 (1977).

[31] Hughes, T.J.R., M .Cohen and M. Haroun, "Reduced and Selective Integration Techniques in the Finite Element Analysis of Plates", Nuclear Engineering and Design, Volume 46, p. 203-222 (1978).

[32] Hughes, T.J.R., and M. Cohen, "The Heterosis Finite Element for Plate Bending", Computers & Structures, Volume 9, p. 445-450 (1978).

[33] Hughes, T.J.R., "Generalization of Selective Integration Procedures to Anisotropic and Nonlinear Media", International Journal for Numerical Methods in Engineering, Volume 15, p. 1413-1418 (1980).

[34] Hughes, T.J.R., and W.K. Liu, "Nonlinear Finite Element Analysis of Shells: Part I - Three-Dimensional Shells", Computer Methods in Applied Mechanics and Engineering, Volume 26, p. 331-362 (1981).

[35] Hughes, T.J.R., and T.E. Tezduyar, "Finite Elements Based Upon Mindlin Plate Theory with Particular Reference to the Four-Node Bilinear Isoparametric Element", Journal of Applied Mechanics, ASME, Volume 48, p. 587-596 (1981).

[36] Irons, B.M., "The SemiLoof Shell Element', in Finite Elements for Thin Shells and Curved Members, John Wiley & Sons, New York, p. 197-221 (1976).

[37] Kanoknukulchai, W., "A Simple and Efficient Finite Element for General Shell Analysis", International Journal for Numerical Methods in Engineering, Volume 14, p. 179-200 (1979).

[38] Lee, S.W. and T.H.H. Pian, "Improvement of Plate and Shell Finite Elements by Mixed Formulations", AIAA Journal, Volume 16, p. 29-34 (1978).

[39] Liu, W.K., J.S.J. Ong and R.A. Uras, "Finite Element Stabilization Matrices - A Unification Approach", Computer Methods in Applied Mechanics and Engineering (to appear).

[40] MacNeal, R.H., "A Simple Quadrilateral Shell Element" Computers & Structures, Volume 8, p. 175-183 (1978).

[41] MacNeal, R.H., "Derivation of Element Stiffness Matrices by Assumed Strain Distributions", Nuclear Engineering and Design, Volume 70, p. 3-12 (1982).

[42] MacNeal, R.H. and R.L. Harder, "A Proposed Standard Set of Problems to Test Finite Element Accuracy", Finite Elements in Analysis and Design, Volume 1, No. 1 (1985).

[43] MACSYMA Reference Manual, Version 9, Massachusetts Institute of Technology, Cambridge (1977).

[44] Malkus, D.S. and T.J.R. Hughes, "Mixed Finite Element Methods - Reduced and Selective Integration Techniques: A Unification of Concepts", Computer Methods in Applied Mechanics and Engineering, Volume 15, p. 63-81 (1978).

[45] Morley, L.S.D., Skew Plates and Structures, Pergamon Press, London (1963).

[46] Noor, A.K. and J.M. Peters, "Mixed and Reduced/Selective Integration Displacement Models for Nonlinear Analysis of Curved Beams", International Journal for Numerical Methods in Engineering, Volume 17, p. 615-631 (1981).

[47] Noor, A.K. and C.M. Andersen, "Mixed Models and Reduced/Selective Integration Displacement Models for Nonlinear Shell Analysis", International Journal for Numerical Methods in Engineering, Volume 18, p. 1429-1454 (1982).

[48] Parisch, H., "A Critical Survey of the 9-Node Degenerated Shell Element with Special Emphasis on Thin Shell Application and Reduced Integration", Computer Methods in Applied Mechanics and Engineering, Volume 20, p. 323-350 (1979).

[49] Park, K.C. and G.M. Stanley, "A Curved C^{o} Shell Element Based on Assumed Natural-Coordinate Strains", Journal of Applied Mechanics, Volume 53, p. 278-290 (1986).

[50] Pian, T.H.H., "Derivation of Element Stiffness Matrices by Assumed Stress Distributions", AIAA Journal, Volume 2, p. 1333-1336 (1964).

[51] Pian, T.H.H., "Variational Principles for Incremental Finite Element Methods", Journal of the Franklin Institute, Volume 302, p. 473-488 (1976).

[52] Pian, T.H.H., "Recent Advances in Hybrid/Mixed Finite Elements", Proceedings of International Conference on Finite Element Methods, Shanghai, China (1982).

[53] Pian, T.H.H., D.P. Chen and D. Kang, "A New Formulation of Hybrid/Mixed Finite Element", Computers & Structures, Volume 16, p. 81-87 (1983).

[54] Pian, T.H.H. and D.P. Chen, "On the Suppression of Zero Energy Deformation Modes", International Journal for Numerical Methods in Engineering, Volume 19, p. 1741-1752 (1983).

[55] Pinsky, P.M. and J. Jang, "An Elastoplastic Shell Element Based on Assumed Covariant Strain Interpolations", Journal of Engineering Mechanics ASCE Division, Volume 114, No. 6, p. 1045-1062 (1988).

[56] Pugh, E.D.L., E. Hinton and O.C. Zienkiewicz, "A Study of Quadrilateral Plate Bending Elements with Reduced Integration", International Journal for Numerical Methods in Engineering, Volume 12, p. 1059-1079 (1978).

[57] Rhiu, J.J. and S.W. Lee, "A New Mixed Formulation for Finite Element Analysis of Thin Shell Structures", International Journal for Numerical Methods in Engineering, Volume 24, p. 581-604 (1987).

[58] Rhiu, J.J. and S.W. Lee, "A Nine Node Finite Element for Analysis of Geometrically Nonlinear Shells" (to appear).

[59] Saleeb, A.F., and T.Y. Chang, "On the Hybrid/Mixed Formulation of C Curved Beam Elements", Computer Methods in Applied Mechanics and Engineering, Volume 60, p. 95-121 (1987).

[60] Saleeb, A.F. and T.Y. Chang, "An Efficient Quadrilateral Element for Plate Bending Analysis", International Journal for Numerical Methods in Engineering, Volume 24, p. 1123-1155 (1987).

[61] Saleeb, A.F., T.Y. Chang and W. Graf, "A Quadrilateral Shell Element Using a Mixed Formulation", International Journal for Numerical Methods in Engineering, Volume 26, No. 5, p. 787-803 (1987).

[62] Sawamiphakdi, K., "Large Deformation and Post-Buckling Analysis of Shells by Finite Element Method", PhD Dissertation, Dept of Civil Engineering, University of Akron, Akron, Ohio (1982).

[63] Spilker, R.L. and N.I. Munir, "The Hybrid-Stress Model for Thin Plates", International Journal for Numerical Methods in Engineering, Volume 15, p. 1239-1260 (1980).

[64] Spilker, R.L., S.M. Maskeri and E. Kania, "Plane Isoparametric Hybrid-Stress Elements : Invariance and Optimal Sampling", International Journal for Numerical Methods in Engineering, Volume 17, p. 1469-1496 (1981).

[65] Stanley, G.M., K.C. Park and T.J.R. Hughes, "Continuum-Based Resultant Shell Elements", in Finite Element Methods for Plate and Shell Structures, Volume 2, Pineridge Press, Swansea, p. 1-45 (1986).

[66] Stolarski, H. and T. Belytschko, "Membrane Locking and Reduced Integration for Curved Elements", Journal of Applied Mechanics, Volume 49, p. 172-176 (1982).

[67] Tang, L.M., W.J. Chen and Y.X. Liu, "String Net Function Approximation and Quasi-Conforming Technique", in Hybrid and Mixed Finite Element Methods, John Wiley & Sons, p. 173-188 (1983).

[68] Tessler, A. and T.J.R. Hughes, "An Improved Treatment of Transverse Shear in the Mindlin-Type Four-Node Quadrilateral Element", Computer Methods in Applied Mechanics and Engineering, Volume 39, p. 311-335 (1983).

[69] Tessler, A. and T.J.R. Hughes, "A Three-Node Mindlin Plate Element with Improved Transverse Shear", Computer Methods in Applied Mechanics and Engineering, Volume 50, p. 71-101 (1985).

[70] Washizu, K., Variational Methods in Elasticity and Plasticity, 3rd ed., Pergamon Press, Oxford (1982).

[71] Wilson, E.L., R.L. Taylor, W. Doherty and J. Ghaboussi, "Incompatible Displacement Models", in Numerical and Computer Methods in Structural Mechanics, Academic Press Inc., New York, p. 43-57 (1973).

[72] Zienkiewicz, O.C., R.L. Taylor and J.M. Too, "Reduced Integration Technique in General Analysis of Plates and Shells", International Journal for Numerical Methods in Engineering, Volume 3, p. 275-290 (1971).

[73] Zienkiewicz, O.C., The Finite Element Method, 3rd ed., McGraw-Hill, London (1977).

APPENDICES

APPENDIX A

Nonlinear Problem Set Load Step Information

Section	Number of Equal Steps	From Load	To Load
7.4	6	0.00	0.15
	15	0.15	0.30
	30	0.30	0.45
7.5	16	0.00	4.00
7.6	8	0.00	2.00
	4	2.00	2.20
	0.01 increments to snap-through		
7.7	2	0.00	1.00
	8	1.00	3.00
	2	3.00	4.00
7.8	20	0.00	3.7E-04
7.9	20	0.00	0.474
7.10	20	0	500
7.11	10 *	0.00	1.85E-04

* NOTE : Q9-URI was unstable at this load level increment. A solution was finally obtained when load was further subdivided into 30 equal steps.

APPENDIX B

Nonlinear Problem Set Solution Time Information

Section	Element (mesh)	DOF	Total No. Iterations	CPU time	Ratio
7.4	Q9-URI (2)	60	250	205 sec	1.00
	SHELM5 (4)	60		413 sec	2.01
	SHELM5 (6)	90	252	569 sec	2.78
	SHELM9 (2)	60	252	618 sec	3.01
7.5	Q9-URI (3)	90	47	63 sec	1.00
	SHELM5 (6)	90	38	101 sec	1.60
	SHELM9 (3)	90	38	165 sec	2.62
7.7	Q9-URI (4x4)	328	38	297 sec	1.00
	SHELM9 (4x4)	328	26	643 sec	2.16
7.8	Q9-URI (5x5)	550	---	---	---
	SHELM5 (5x5)	275	45	8.65 min	
	SHELM9 (5x5)	550	33	24.6 min	
7.9	Q9-URI (5x5)	550	---	---	---
	SHELM5 (7x7)	525	43	20.8 min	
	SHELM9 (5x5)	550	34	25.1 min	
7.10	Q9-URI (5x5)	550	0	---	---
	SHELM5 (7x7)	525	0	5.6 min	
	SHELM9 (5x5)	550	0	9.3 min	

REPORT DOCUMENTATION PAGE

Form Approved
OMB No. 0704-0188

1. AGENCY USE ONLY (*Leave blank*)	2. REPORT DATE	3. REPORT TYPE AND DATES COVERED
	December 1991	Final Contractor Report

4. TITLE AND SUBTITLE

A Geometric Nonlinear Degenerated Shell Element Using a Mixed Formulation With Independently Assumed Strain Fields

5. FUNDING NUMBERS

WU-505-63-5B
G-NAG3-307

6. AUTHOR(S)

Wiley E. Graf

7. PERFORMING ORGANIZATION NAME(S) AND ADDRESS(ES)

University of Akron
Department of Civil Engineering
Akron, Ohio 44325-3905

8. PERFORMING ORGANIZATION REPORT NUMBER

None

9. SPONSORING/MONITORING AGENCY NAMES(S) AND ADDRESS(ES)

National Aeronautics and Space Administration
Lewis Research Center
Cleveland, Ohio 44135-3191

10. SPONSORING/MONITORING AGENCY REPORT NUMBER

NASA CR-189086

11. SUPPLEMENTARY NOTES

Project Manager, C.C. Chamis, Structures Division, NASA Lewis Research Center, (216) 433-3252. Report submitted as a dissertation in partial fulfillment of the requirements for the degree Doctor of Philosophy to the University of Akron, Akron, Ohio in 1989.

12a. DISTRIBUTION/AVAILABILITY STATEMENT

Unclassified - Unlimited
Subject Category 39

12b. DISTRIBUTION CODE

13. ABSTRACT (*Maximum 200 words*)

A mixed formulation is chosen to overcome deficiencies of the standard displacement-based shell model. Element development is traced from the incremental variational principle on through to the final set of equilibrium equations. Particular attention is paid to developing specific guidelines for selecting the optimal set of strain parameters. Included is a discussion of constraint index concepts and their predictive capability related to locking. Performance characteristics of the elements are assessed in a wide variety of linear and nonlinear plate/shell problems. Despite limiting the study to geometric nonlinear analysis, a substantial amount of additional insight concerning the finite element modelling of thin plate/shell structures is provided. For example, in nonlinear analysis, given the same mesh and load step size, mixed elements converge in fewer iterations than equivalent displacement-based models. It is also demonstrated that, in mixed formulations, lower order elements are preferred. Additionally, meshes used to obtain accurate linear solutions do not necessarily converge to the correct nonlinear solution. Finally, a new form of locking was identified associated with employing elements designed for biaxial bending in uniaxial bending applications.

14. SUBJECT TERMS	15. NUMBER OF PAGES
Variational principle; Plate; Shells; Multifield beams end-shears; Pinched cylinder; In-plate; Bending; Sample cases; Locking	124
	16. PRICE CODE A06

17. SECURITY CLASSIFICATION OF REPORT	18. SECURITY CLASSIFICATION OF THIS PAGE	19. SECURITY CLASSIFICATION OF ABSTRACT	20. LIMITATION OF ABSTRACT
Unclassified	Unclassified	Unclassified	